Research Article

Magnetic Resonance in Chemistry

Received: 31 March 2010 Revised: 17 May 2010 Accepted: 20 May 2010 Published online in Wiley Online Library: 29 June 2010

(wileyonlinelibrary.com) DOI 10.1002/mrc.2635

New perspectives in the PAW/GIPAW approach: J_{P-O-Si} coupling constants, antisymmetric parts of shift tensors and NQR predictions†

Christian Bonhomme,[a]* Christel Gervais,[a] Cristina Coelho,[b] Frédérique Pourpoint,[a] Thierry Azaïs,[a] Laure Bonhomme-Coury,[a] Florence Babonneau,[a] Guy Jacob,[c] Maude Ferrari,[d] Daniel Canet,[d] Jonathan R. Yates,[e] Chris J. Pickard,[f] Siân A. Joyce,[g] Francesco Mauri[h] and Dominique Massiot[i]

In 2001, Pickard and Mauri implemented the gauge including projected augmented wave (GIPAW) protocol for first-principles calculations of NMR parameters using periodic boundary conditions (chemical shift anisotropy and electric field gradient tensors). In this paper, three potentially interesting perspectives in connection with PAW/GIPAW in solid-state NMR and pure nuclear quadrupole resonance (NQR) are presented: (i) the calculation of *J* coupling tensors in inorganic solids; (ii) the calculation of the antisymmetric part of chemical shift tensors and (iii) the prediction of ^{14}N and ^{35}Cl pure NQR resonances including dynamics. We believe that these topics should open new insights in the combination of GIPAW, NMR/NQR crystallography, temperature effects and dynamics. Points (i), (ii) and (iii) will be illustrated by selected examples: (i) chemical shift tensors and heteronuclear $^2J_{P-O-Si}$ coupling constants in the case of silicophosphates and calcium phosphates [$Si_5O(PO_4)_6$, SiP_2O_7 polymorphs and α-$Ca(PO_3)_2$]; (ii) antisymmetric chemical shift tensors in cyclopropene derivatives, C_3X_4 (X = H, Cl, F) and (iii) ^{14}N and ^{35}Cl NQR predictions in the case of RDX ($C_3H_6N_6O_6$), β-HMX ($C_4H_8N_8O_8$), α-NTO ($C_2H_2N_4O_3$) and $AlOPCl_6$. RDX, β-HMX and α-NTO are explosive compounds.

Supporting information may be found in the online version of this article.

Keywords: solid-state NMR; GIPAW; *J* tensors; antisymmetric parts of tensors; NQR

Introduction

Recent improvements in solid-state NMR methodology and instrumentation (ultrahigh field up to 23.5 T, $\nu_0(^1H) = 1$ GHz, ultrafast magic angle spinning (MAS) up to 70 kHz, improved homonuclear and heteronuclear decoupling/recoupling schemes, etc.) have led to a better description of organic/inorganic structures in terms of NMR interactions and tensorial properties.[1–3] Various quantum mechanical (QM) approaches can be used for the calculations of spectroscopic parameters.[4]

A major breakthrough was achieved in 2001 by Pickard and Mauri,[5] with the implementation of the projected augmented wave/gauge including projected augmented wave (PAW/GIPAW) protocol. Avoiding any cluster approximation, PAW/GIPAW allows first-principles calculations of chemical shift anisotropy (FPC-CSA) and electric field gradient (EFG) tensors for all active nuclei in a given structure by using density functional theory (DFT), pseudopotentials and all-electron Hamiltonians. Since the introduction of GIPAW, a large panel of applications of the GIPAW/NMR combination has been reported in the literature. Among others, the fields of organic crystals and H-bonding, inorganic structures, biocompatible materials, geomaterials, carbon nanotubes, etc. have been investigated so far.[6] GIPAW is now recognized as a valuable tool for definite assignments of spectra, *a priori* predictions of NMR data and NMR crystallography.[7] Very recently, the combination of crystal structure prediction (CSP),[8] GIPAW calculations and high-resolution solid-state NMR has culminated in the *ab initio* structure determination of a small organic molecule (thymol).[9]

* *Correspondence to: Christian Bonhomme, Laboratoire de Chimie de la Matière Condensée, Université Pierre et Marie Curie, Paris 06, CNRS UMR 7574, Collège de France, 11 place M. Berthelot, 75005 Paris, France. E-mail: christian.bonhomme@upmc.fr*

† *Paper published as part of the Quantum-Chemical Calculations and their applications special issue.*

a *Laboratoire de Chimie de la Matière Condensée, Université Pierre et Marie Curie, Paris 06, CNRS UMR 7574, Collège de France, 75005 Paris, France*

b *Institut des Matériaux de Paris Centre, Université Pierre et Marie Curie, Paris 06, CNRS FR 2482, Collège de France, 75005 Paris, France*

c *SME, Centre de Recherches du Bouchet, 91710 Vert le Petit, France*

d *Méthodologie RMN (CRM2, UMR 7036 CNRS – Nancy-Université), Faculté des Sciences et Technologies, 54506 Vandoeuvre-lès-Nancy, Cedex, France*

e *Department of Materials, University of Oxford, Oxford OX1 3PH, UK*

f *Department of Physics and Astronomy, University College London, London WC1E 6BT, UK*

g *Tyndall National Institute, Lee Maltings, Cork, Ireland*

h *Laboratoire de Minéralogie Cristallographie UMR CNRS 7590, UPMC, Campus Boucicaut, 75015 Paris, France*

i *CNRS UPR 3079 CEMHTI, Université d'Orléans, 45071 Orléans Cedex, France*

The following question can be raised: what are the new potentialities of GIPAW to be explored as a user of the GIPAW/NMR combination? From our point of view, three (partial) answers can be given:

1. Almost all GIPAW published data are related to CSA and EFG tensors (including absolute orientation of both tensors in the crystal frame). In solid-state NMR, four fundamental interactions have to be considered for diamagnetic systems: CSA, EFG, *D* (direct dipolar coupling) and *J* (indirect nuclear spin–spin coupling). The first future trend of PAW/GIPAW could be the routine calculation of *J* coupling tensors in solids, as sophisticated experimental measurements of *J* constants have been made recently.[10] In 2007, Joyce *et al*.[11] have proposed a theoretical framework for the calculation of *J* interaction using the PAW method. Beyond the initial validation, only a small number of applications have been published to date, all involving molecular crystals.[12] Obviously, more calculations are needed to assess the accuracy of the approach, especially in the field of inorganic materials.
2. As shown by the contribution of Buckingham and Malm,[13] it has been understood that the magnetic shielding tensor should be represented, in general, by an asymmetric second-rank tensor with nine independent components. GIPAW calculations automatically provide the full shielding tensors, including its antisymmetric components, i.e. $\sigma^{\text{anti}} = 1/2(\sigma - \sigma^{t})$, where σ^{t} stands for the transpose of σ. The antisymmetric components are usually safely neglected, as they affect the NMR spectrum in second order only.[14] However, σ^{anti} can be involved in relaxation times T_1 and T_2, and some relevant data are available in the literature.[15] From a spectroscopic point of view, Wi *et al*.[16] have shown theoretically that cross-correlation Hamiltonians $H^{(2)}_{Q,\sigma^{\text{anti}}}$ could lead to the direct detection of the antisymmetric shift components. Very recently, Harris *et al*.[17] have reported the first attempts to measure $\mathbf{J}^{\text{anti}}$ components in tin derivatives. Therefore, it seems promising to investigate more carefully the σ^{anti} parts of the GIPAW shielding tensors, as they are obtained without any extra computational time.
3. GIPAW calculations are generally performed at 0 K. The role of temperature, vibrational motions and dynamics on the observed spectroscopic parameters is still a debated issue[18,19] and only a few publications have examined the impact of local dynamics and 0 K GIPAW data.[20] It is well known that pure NQR resonances are highly sensitive to temperature and dynamics, including librations and hindered internal rotations of molecules.[21] Therefore, the PAW-calculated C_Q and η_Q (quadrupolar constant and asymmetry parameter) values can be used for the calculation of NQR resonances: these resonances can be considered as limits at 0 K of low-temperature NQR data. In that sense, PAW acts here as a predictive tool.[22] On the other hand, NQR spectroscopy offers a real opportunity to monitor the explicit effect of temperature in future PAW/GIPAW developments.

In this article, we will illustrate points 1, 2 and 3 by developing the following topics:

1. Silicophosphate phases, including $Si_5O(PO_4)_6$ and SiP_2O_7 polymorphs[23] are fully characterized by ^{29}Si, ^{31}P NMR and GIPAW calculations. $|^2J_{P-O-Si}|$ coupling constants are measured (with reasonable precision) by ^{31}P–^{29}Si MAS-J-INEPT experiments[24] and compared with GIPAW calculations. It has to be stressed that $Si_5O(PO_4)_6$ acted as a standard for the implementation of *J* calculations in PAW.[11] To the best of our knowledge, these calculated heteronuclear *J* data are the first for inorganic derivatives using the PAW approach (it has to be noted that recent work using cluster models to compute *J* constants has been published).[10b,25] Moreover, the estimation of the accuracy of the ^{31}P GIPAW calculated data for silico- and calcium phosphates is given.
2. Antisymmetric (AS) shift components have been rarely reported in the literature. GIPAW components are calculated for three cyclopropene derivatives (C_3X_4: X = H, Cl, F), as experimental estimations are available.[15,26] In the past, several QM approaches have been used for cyclopropene analyses and some discrepancies between sets of calculated data were observed. It is demonstrated that GIPAW-calculated values are in very good agreement with experimental data.
3. ^{14}N quadrupolar and shift parameters are calculated using PAW/GIPAW for RDX ($C_3H_6N_6O_6$), β-HMX ($C_4H_8N_8O_8$) and α-NTO ($C_2H_2N_4O_3$) (explosive compounds).[27] The calculated NQR resonances are compared with extrapolated low- temperature NQR frequencies, taking into account librations of molecules empirically. ^{35}Cl quadrupolar and shift parameters in $AlOPCl_6$ are calculated as well by GIPAW. The experimental 'fading out' of the NQR resonances is interpreted in terms of hindered internal rotations of the PCl_3 and $AlCl_3$ groups. In other words, GIPAW predictions and local dynamics are necessary for a full understanding of the NQR data.

Experimental

Syntheses

$Si_5O(PO_4)_6$: 5.74 g (27.5 mmol) of tetraethoxysilane $Si(OCH_2CH_3)_4$ (tetraethylorthosilicate, TEOS, purchased from Fluka) was added to 3.81 g of H_3PO_4 (85%) (33.0 mmol, purchased from Aldrich). The inhomogeneous gel was vigorously stirred until a very viscous liquid was obtained. After 48 h stirring, the vessel was opened for 48 h to air. The obtained powder was heated at 100 °C for 48 h for further drying. The obtained xerogel was heated at 800 °C for 2 h. $Si_5O(PO_4)_6$ was detected as the main phase by powder X-ray diffraction (Joint Committee on Powder Diffraction Standards (JCPDS): 70–2071). Amorphous silica was obtained as a side product.[23b] Polymorphs of SiP_2O_7: after the dissolution of 0.11g (0.46 mmol) of $NiCl_2.6H_2O$ in ethanol (for shortening of $T_1(^{31}P)$ and $T_1(^{29}Si)$ relaxation times), 17.61 g (179.7 mmol) of phosphoric acid (H_3PO_4 85%) was added, followed by 9.33 g (44.8 mmol) of TEOS. A gel was obtained immediately at room temperature. The powder was first heated at 100 °C during 48 h and then at 1000 °C for 4 h. The obtained mixture contains the following phases: $Si_5O(PO_4)_6$, SiP_2O_7 polymorphs: monoclinic AIII, JCPDS: 72–0647, monoclinic AIV, JCPDS: 70–2245, hexagonal 1, JCPDS: 82–1061 and tetragonal, JCPDS: 22–1320 (Fig. 1c). $AlOPCl_6$: the synthesis proposed by Burford *et al*.[28] has been repeated (reaction of $OPCl_3$ and $AlCl_3$ in CH_2Cl_2). As $AlOPCl_6$ is highly sensitive to moisture, NMR rotors were packed in a dried glove box.

Solid-state NMR spectroscopy

All experiments were performed on Bruker AVANCE II 300, 400 and 750 spectrometers using double and triple resonance Bruker MAS probes. $Si_5O(PO_4)_6$ (Fig. 1a and b): ^{31}P MAS, 7.04 T, $\nu_0(^{31}P) = 121.50$ MHz, rotor diameter (Ø) = 4 mm, MAS frequency

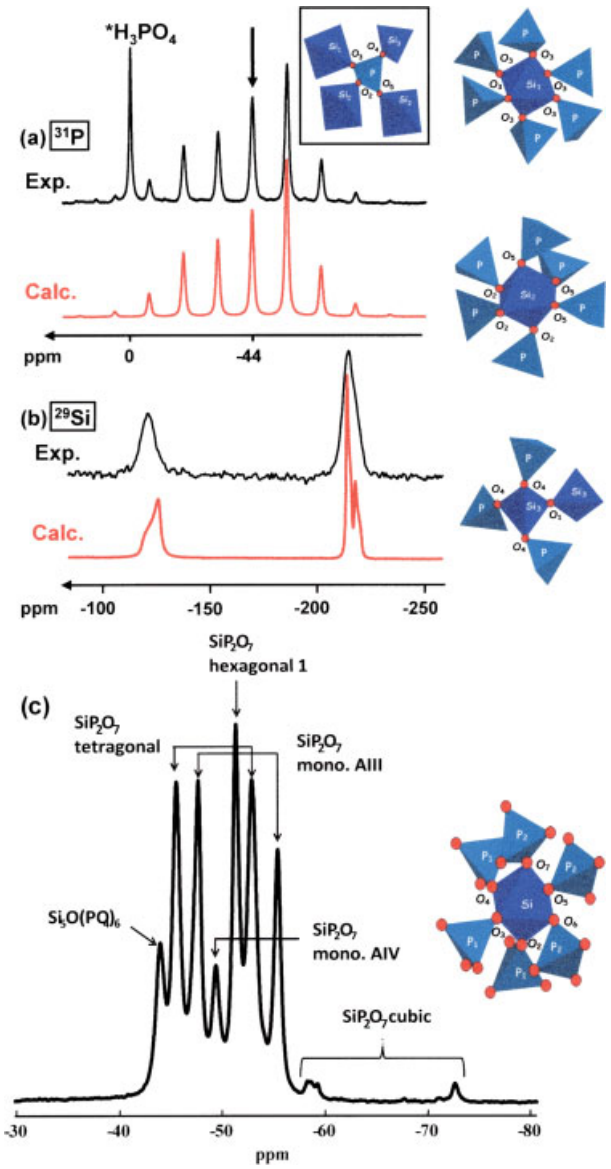

Figure 1. (a) ^{31}P slow MAS NMR spectrum of $Si_5O(PO_4)_6$; (b) ^{31}P–^{29}Si CP static spectrum of $Si_5O(PO_4)_6$ and (c) ^{31}P fast MAS spectrum of a mixture including $Si_5O(PO_4)_6$ and SiP_2O_7 polymorphs. All NMR parameters are given in th Experimental section. The calculated spectra correspond to GIPAW calculations given in Table 1.

(ν_{rot}) = 2 kHz, number of scans (NS) = 124, recycle delay (RD) = 60 s with presaturation, $t_{90°}(^{31}P)$ = 3.0 µs; ^{31}P–^{29}Si CP static, 7.04 T, $\nu_0(^{31}P)$ = 121.50 MHz, $\nu_0(^{29}Si)$ = 59.63 MHz, Ø = 4 mm, triple resonance probe, NS = 5160, RD = 60 s with presaturation, $t_{90°}(^{31}P)$ = 5.0 µs, contact time = 40 ms, CW {^{31}P} decoupling = 47.2 kHz. Polymorphs of SiP_2O_7 (Figs 1c and 5): ^{31}P MAS, 7.04 T, $\nu_0(^{31}P)$ = 121.50 MHz, Ø = 4 mm, ν_{rot} = 14 kHz, NS = 8, RD = 10 s, $t_{90°}(^{31}P)$ = 3.9 µs. ^{31}P–^{29}Si MAS-J-INEPT,[24] 7.04 T, $\nu_0(^{31}P)$ = 121.50 MHz, $\nu_0(^{29}Si)$ = 59.63 MHz, Ø = 4 mm, ν_{rot} = 14 kHz, triple resonance probe, NS = 1776, dummy scans (DS) = 16, RD = 7 s, $t_{90°}(^{31}P)$ = 3.9 µs, $t_{90°}(^{29}Si)$ = 4.5 µs, fixed τ = 12.85 ms, variable τ' (see Ref. [24] for pulse scheme and experimental details). $AlOPCl_6$ (Fig. 10a and b): ^{31}P MAS, 17.6 T, $\nu_0(^{31}P)$ = 303.6 MHz, Ø = 4 mm, ν_{rot} = 5 kHz, NS = 64, RD = 10 s. ^{27}Al MAS, 17.6 T, $\nu_0(^{27}Al)$ = 195.46 MHz, Ø = 4 mm, ν_{rot} = 3 kHz, NS = 128, RD = 1 s.

Chemical shifts references for all the tables: ^{31}P: 85% aqueous H_3PO_4. ^{27}Al: aq. $Al(NO_3)_3$ 1 M. ^{1}H, ^{13}C, ^{29}Si: TMS. ^{15}N: nitromethane. ^{35}Cl: NaCl (solid). ^{19}F: $CFCl_3$.

Experimental errors for ^{31}P and ^{29}Si NMR data are estimated to be 0.05 ppm. The simulations of all spectra were performed by using the (QUASAR) module in the DMFit platform.[29]

Computational method

The calculations were performed within Kohn–Sham DFT with the GIPAW[5] approach for computing magnetic resonance parameters. The PARATEC code[30] was used to calculate the shielding and EFG, and a developer's version of the CASTEP code[31] to compute *J* coupling.[11] In each case, the PBE generalized gradient approximation[32] was used and the valence electrons were described by norm-conserving pseudopotentials[33] in the Kleinman and Bylander[34] form. The core definition for O, N, C and F is $1s^2$ and $1s^22s^22p^6$ for P, Si, Al, Cl and Ca. The core radii are 1.1 a.u. for F, 1.2 a.u. for H, 1.45 a.u. for Ca, 1.5 a.u. for O, 1.6 a.u. for C, 1.7 a.u. for Si, 1.8 a.u. for Al, 1.9 a.u. for Cl and 2.0 a.u. for P. The wave functions are expanded on a plane-wave basis set with a kinetic energy cut-off of 80 Ry. The crystalline structure is described as an infinite periodic system using periodic boundary conditions. The NMR calculations were performed using experimental geometries for silicophosphates,[35] α-$Ca(PO_3)_2$,[36] $C_3H_6N_6O_6$ (RDX),[37] $C_4H_8N_8O_8$ (β-HMX),[38] $C_2H_2N_4O_3$ (α-NTO)[39] and $AlOPCl_6$.[28] In the case of the hexagonal form of SiP_2O_7[40] and α-$Ca(PO_3)_2$, a geometry optimization was carried out starting from the experimental one and allowing the positions of all atoms to relax using DFT calculations. H-relaxed structure was used only in the case of α-NTO. Cyclopropene and tetrafluorocycloprene theoretical geometries were used,[41] and atomic positions were additionally relaxed using DFT calculations. For tetrachlorocycloprene, the initial geometry of tetrafluorocycloprene was used with C–Cl distances modified to fit with known values. The cyclopropene-derived molecules are isolated in the unit cell. The CIF files for the three corresponding structures are presented in Supporting Information. The *J* coupling is obtained by considering the perturbation between the magnetic moment of the chosen atom and all other atoms in the system. The perturbation breaks the translational symmetry of the system, and for small unit cells it is necessary to study a supercell of the primitive cell to inhibit the interaction of periodically repeated images of the perturbing site. The following sizes of supercells were used: $Si_5O(PO_4)_6$ – 2 × 2 × 1, SiP_2O_7: AIII – 2 × 2 × 1, AIV, 2 × 1 × 2, hexogonal 1 – 2 × 2 × 1.

The isotropic chemical shift δ_{iso} is defined as $\delta_{iso} = -[\sigma - \sigma^{ref}]$, where σ is the isotropic shielding and σ^{ref} is the isotropic shielding of the same nucleus in a reference system as previously described.[42–45] Diagonalization of the symmetrical part of the calculated tensor provides its principal components δ_{11}, δ_{22} and δ_{33} defined such as $|\delta_{33} - \delta_{iso}| \geq |\delta_{11} - \delta_{iso}| \geq |\delta_{22} - \delta_{iso}|$ and $\delta_{iso} = 1/3(\delta_{11} + \delta_{22} + \delta_{33})$. The CSA parameters are defined by $\Delta_{CSA} = \delta_{33} - \delta_{iso}$ and $\eta_{CSA} = |(\delta_{22} - \delta_{11})/\Delta_{CSA}|$. The AS ($\delta_{12}$, δ_{13}, δ_{23}) shift components are calculated as well. In connection with relaxation studies, *A* (antisymmetric) and *S* (symmetric) quantities are defined as follows: $A^2 = (\delta_{12})^2 + (\delta_{13})^2 + (\delta_{23})^2$ and $S^2 = (\delta_{CSA})^2(1 + \eta_{CSA}{}^2/3)$, with $\delta_{CSA} = \delta_{33} - 1/2(\delta_{11} + \delta_{22})$. The principal components V_{xx}, V_{yy} and V_{zz} of the EFG tensor, defined as $|V_{zz}| \geq |V_{xx}| \geq |V_{yy}|$, are obtained by diagonalization of the tensor. The quadrupolar interaction can then be characterized by the

quadrupolar coupling constant C_Q and the asymmetry parameter η_Q, which are defined as $C_Q = eQV_{zz}/h$ and $\eta_Q = |(V_{yy} - V_{xx})/V_{zz}|$, where e is the proton charge, h is the Planck constant and Q is the quadrupole moment of the considered nucleus. For the J principal components, $|J_{33} - J_{iso}| \geq |J_{11} - J_{iso}| \geq |J_{22} - J_{iso}|$, and $J_{iso} = 1/3(J_{11} + J_{22} + J_{33})$. For the purposes of analysis, J can be expressed as the sum of four (Ramsey) contributions[11]: the Fermi-contact (FC), spin-dipolar (SD), paramagnetic orbital (PARA) and diamagnetic orbital (DIA) terms. This decomposition into four Ramsey contributions stands for the isotropic part of J. For the full J tensor (including anisotropy), a fifth component must be taken into account: FC/SD. This term contributes to the anisotropy only (the FC term contributes to the isotropy only). The remaining terms give contribution to both J isotropy and anisotropy. J_{aniso} is given by $J_{33} - 1/2(J_{11} + J_{22})$. It is worth noting that the program outputs all three tensors in the crystal axis system. Absolute orientation in the molecular frame of the shielding, EFG and J tensors, as well as their relative orientations, can therefore be obtained.

Results and Discussion

Silicophosphate derivatives: toward the calculation of *J* coupling constants in inorganic materials

Recently, we have proposed to combine FPC-NMR parameters and multidimensional NMR experiments for full assignment of the various forms of biocompatible $Ca(PO_3)_2$ (β- and γ-polymorphs).[46] As shown in the case of $Ca(PO_3)_2$, the FPC-NMR approach opens novel insights into the full understanding of NMR data in the frame of biocompatible materials. To the best of our knowledge, only a few GIPAW calculations of ^{31}P NMR parameters have been published so far in the literature.[47] The goal of this section is to focus on three crucial points related to the accuracy of the calculated parameters, the extraction of full tensorial sets of data and the calculation of heteronuclear J coupling constants. In order to illustrate these points, several silicophosphates (including $Si_5O(PO_4)_6$ and polymorphs of SiP_2O_7) and the newly reported α-$Ca(PO_3)_2$ phase[36] were fully characterized by ^{31}P, ^{29}Si solid-state NMR and the GIPAW approach. Full experimental assignments for ^{29}Si and ^{31}P resonances have been obtained recently by extensive use of one- and two-dimensional (2D) $^{31}P-^{29}Si$ solid-state NMR experiments.[23,24] The crystallographic data for all phases and the NMR data for α-$Ca(PO_3)_2$ were taken from the literature.[36]

The ^{31}P (MAS) and ^{29}Si (static) experimental and calculated spectra (based on the GIPAW data; Table 1) of $Si_5O(PO_4)_6$ are presented in Fig. 1a and b. The $Si_5O(PO_4)_6$ structure exhibits a unique P site connected to sixfold (Si1,Si2) and fourfold coordinated (Si3) silicon atoms (see the insert in Fig. 1a). For Si atoms, Si–O–P bonds involve various O sites (O2 → O5). An excellent agreement is observed between both sets of isotropic data (^{31}P and ^{29}Si). ^{31}P CSA principal values were extracted from slow MAS experiments, whereas the $^{31}P \rightarrow {}^{29}Si$ CP static experimental spectrum is in reasonable agreement with the calculated one (the calculated ^{29}Si CSA are smaller than 6 ppm for all studied silicophosphates; Table 1). A $^{31}P-^{29}Si$ CP

Table 1. Experimental and GIPAW calculated ^{31}P and ^{29}Si parameters for $Si_5O(PO_4)_6$, SiP_2O_7 polymorphs and α-$Ca(PO_3)_2$

		δ_{iso} (ppm)		δ_{11} (ppm)		δ_{22} (ppm)		δ_{33} (ppm)	
Phase	Sites	Experimemtal	Calculated	Experimemtal	Calculated	Experimemtal	Calculated	Experimemtal	Calculated
$Si_5O(PO_4)_6$	P	−44.1	−43.9	−73.6	−76.8	−53.8	−52.9	−4.5	−2.1
	Si_2	−213.5	−213.8	–	−212.9	–	−212.9	–	−215.5
	Si_1	−217.3	−217.9	–	−216.8	–	−216.8	–	−220.1
	Si_3	−119.3	−122.9	–	−125.6	–	−125.6	–	−117.5
SiP_2O_7 III tetragonal	P_1	−45.5	–	−74.1	–	−64.5	–	−2.5	–
	P_2	−52.9	–	−88.9	–	−72.2	–	2.7	–
	Si	−212.8	–	–	–	–	–	–	–
SiP_2O_7 AIII monoclinic	P_1	−47.6	−47.7	−79.7	−79.5	−64.7	−65.6	1.8	1.9
	P_2	−55.3	−55.5	−91.2	−92.8	−74.6	−74.7	0.2	0.7
	Si	−215.5	−215.0	–	−217.1	–	−216.1	–	−210.8
SiP_2O_7 AIV monoclinic	P_1	−47.4	−47.4	−76.6	−79.3	−76.6	−75.8	11.3	11.3
	P_2	−49.5	−49.7	−85.3	−83.9	−61.4	−62.8	−1.6	−4.0
	Si	−215.5	−215.6	–	−217.9	–	−216.6	–	−212.1
SiP2O7 hexagonal 1	P_1	−51.3	−57.0	−90.9[b]	−84.8	−90.0	−85.5	26.3	−0.8
	P_2	−51.3	−57.1	−90.9	−85.2	−90.0	−85.2	26.3	−1.0
	Si	−212.8	−209.9	–	−209.5	–	−209.6	–	−210.7
α-$Ca(PO_3)_2$[a]	P_1	−30.7	−30.6	53.1	64.1	4.7	−1.4	−149.9	−154.6
	P_2	−33.7	−34.3	66.9	68.1	−1.6	4.7	−166.2	−175.6
	P_3	−32.6	−33.3	58.8	59.4	−3.2	−1.2	−153.3	−158.1
	P_4	−34.8	−40.9	57.3	59.6	0.1	0.7	−161.7	−183.0
	P_5	−34.3	−38.7	54.5	57.1	−5.0	−3.6	−152.2	−169.8
	P_6	−32.1	−33.6	62.7	66.6	2.4	7.2	−161.3	−174.6
	P_7	−33.9	−35.1	54.6	65.8	6.7	3.3	−163.0	−174.6
	P_8	−31.0	−30.7	65.1	66.8	−4.0	3.8	−154.2	−162.6

For the definitions of δ_{ii} see the Experimental section.
[a] The experimental data for α-$Ca(PO_3)_2$ are taken from Ref. [36].
[b] From Ref. [48].

static experiment was used in order to supress efficiently any contribution of the amorphous silica impurity (see section on Experimental). Calculated data for sixfold silicon atoms are rarely mentioned in the literature.[6g]

The various polymorphs of SiP_2O_7 (monoclinic AIII, AIV, tetragonal and hexagonal 1 forms – see the Experimental section) represent a strong challenge in terms of FPC. Indeed, all related $\delta_{iso}(^{31}P)$ and $\delta_{iso}(^{29}Si)$ are located in restricted ranges: [−44, −56 ppm] and [−213, −218 ppm], respectively (only sixfold coordinated Si atoms are considered in this case). The ^{31}P fast MAS spectrum of a mixture of $Si_5O(PO_4)_6$ and SiP_2O_7 polymorphs is presented in Fig. 1c. The calculated and experimental ^{31}P and ^{29}Si parameters are presented in Table 1. Both AIII and AIV monoclinic forms are distinguished through P1 and P2 chemical shifts ($\Delta\delta = |\delta_{P1} - \delta_{P2}|$ approximately 8 ppm for AIII and 2 ppm for AIV).[23,24] Again, the calculated values are in excellent agreement with the experimental ones, demonstrating the intrinsic precision of the ^{31}P (and ^{29}Si) GIPAW approach. Moreover, it is important to notice that $\Delta\delta$ is not sufficient to characterize properly the symmetry of a given SiP_2O_7 phase. Indeed, the value for the tetragonal form ($\Delta\delta \sim 7$ ppm) is very close to the value of the AIII form. For the tetragonal form, calculated values could not be obtained, as no complete structure was available in the literature but it is now reasonable to think that the measured and computed values could become a constraint for establishing a reliable structural model.

^{31}P CSA are generally slightly larger for all SiP_2O_7 polymorphs [$P(OSi)_3(OP)$ sites] when compared to $Si_5O(PO_4)_6$ [$P(OSi)_4$ site], as expected from symmetry considerations. The absolute orientations of ^{29}Si and ^{31}P CSA tensors can be extracted, as shown in Fig. 2 for the mono. AIII form. It is demonstrated for all phases that the δ_{33} CSA axes for both Si and P atoms are nearly collinear to the Si···P and P···P directions, respectively. Such structural data lead obviously to novel insights into the structural characterization of phosphate phases. Indeed, tensor information is a key for the in-depth understanding of chemical bonding. Such information should be extracted from 2D NMR experiments in the near future requiring the setting up of devoted experimental schemes.

α-$Ca(PO_3)_2$ can be considered as another challenge for the GIPAW method. Eight distinct P sites are involved. The structure contains two unconnected polyphosphate chains, leading to two groups of P atoms. An incomplete assignment based on ^{31}P MAS-J-INADEQUATE is proposed in Ref [36]. Full assignment was obtained by combining the proposed experimental data and GIPAW calculations (Table 1).

In order to get quantitative insight into the ^{31}P GIPAW predictions, a plot of the calculated $\delta_{iso}(^{31}P)$ calculated *versus* $\delta_{iso}(^{31}P)$ experimental is presented in Fig. 3a for $Si_5O(PO_4)_6$, SiP_2O_7 polymorphs and α-, β- and γ-$Ca(PO_3)_2$ polymorphs.[46] Excluding three values (in grey in Fig. 3a), a linear correlation is observed: this observation proves definitely the accuracy of the ^{31}P GIPAW approach for inorganic materials. The root mean square (rms) error $\sqrt{\frac{1}{N}\sum_{i=1}^{N}(\delta^i_{calc.} - \delta^i_{exp.})}$ (for $N = 19$ here) is 0.70 ppm. It has to be noticed that the calculated data related to P4 and P5 in α-$Ca(PO_3)_2$ show some discrepancy with the experimental one (light gray squares in Fig. 3a). Most interestingly, Weil *et al.*[36] mentioned that the P4–O13–P5 fragment was unusual in terms of bond angle (∼180°) and of the high thermal motion of the bridging O atom. This observation is probably related to the less accurate calculated values for ^{31}P shifts. As already mentioned above, the impact of thermal motion in GIPAW has been seldom addressed in the literature.[18] Some discrepancy is also observed in the case

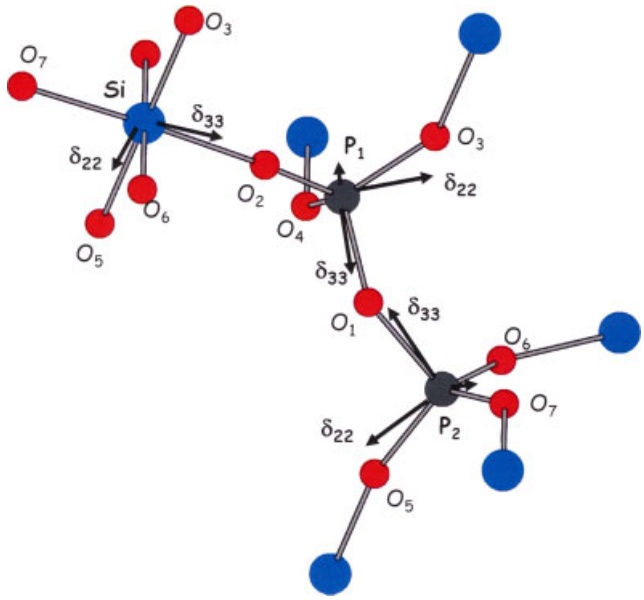

Figure 2. GIPAW calculated ^{29}Si and ^{31}P CSA principal axes for SiP_2O_7, mono. AIII.

of the hexogonal 1 form of SiP_2O_7 (light gray circle in Fig. 3a). In that particular case, the initial crystallographic structure is shown to be highly stressed, and full relaxation of all atoms appeared to be necessary for GIPAW calculations (see the Experimental section). The inaccuracy of the starting XRD model may explain this discrepancy. Although less data is available, a plot of calculated $\delta_{iso}(^{29}Si)$ calculated *versus* $\delta_{iso}(^{29}Si)$ experimental is presented in Fig. 3b for sixfold coordinated Si atoms. A good agreement is obtained (rms error = 0.40 ppm, for $N = 4$). The strongest discrepancy ($\Delta\delta = 3.6$ ppm) is observed for SiP_2O_7 hexogonal 1 as expected (light gray circle in Fig. 3b).

^{17}O solid-state NMR is now considered as a fundamental tool for investigation in the realm of inorganic chemistry.[49] It has been demonstrated that the GIPAW approach is able to accurately calculate the ^{17}O quadrupolar and CSA parameters. However, no experimental data related to P–^{17}O–Si bonds have been published so far. The ^{17}O GIPAW data is presented in Table 2 and as Supporting Information. For $Si_5O(PO_4)_6$, $\delta_{iso}(^{17}O)$ appears to be very sensitive to the chemical nature of the neighboring atoms (P, Si) and also to the coordination of the involved Si atoms (∼40 ppm for pyrosilicate groups, ∼70 ppm for P–O–Si_{IV} groups and ∼100 ppm for P–O–Si_{VI} groups). Close values are obtained for C_Q (∼7 MHz), and small η_Q values ($\leq$0.4) are computed. For SiP_2O_7 polymorphs and α-$Ca(PO_3)_2$ (Supporting Information), P–^{17}O–Si data are comparable to those observed for $Si_5O(PO_4)_6$. P–^{17}O–P fragments are characterized by higher $\delta_{iso}(^{17}O)$, as already mentioned in the literature,[47a,50] and higher C_Q, when compared to P–^{17}O–Si data. Chemical routes are currently checked for the synthesis of ^{17}O-enriched $Si_5O(PO_4)_6$, SiP_2O_7 and calcium phosphate phases in order to perform ^{17}O MAS and MQ-MAS experiments.

There is a contradiction between the Refs [51,52] for the sign of Q in the case of ^{17}O. We adopt here $Q(^{17}O) < 0$, as proposed by Harris and Mann.[53] This negative sign is in agreement with Ref. [54] (a contradiction still remains between this table and Tables 2 and 3 in this last reference).

$Si_5O(PO_4)_6$ has been used recently to validate the use of the PAW approach for the calculation of J coupling in solid materials.[11]

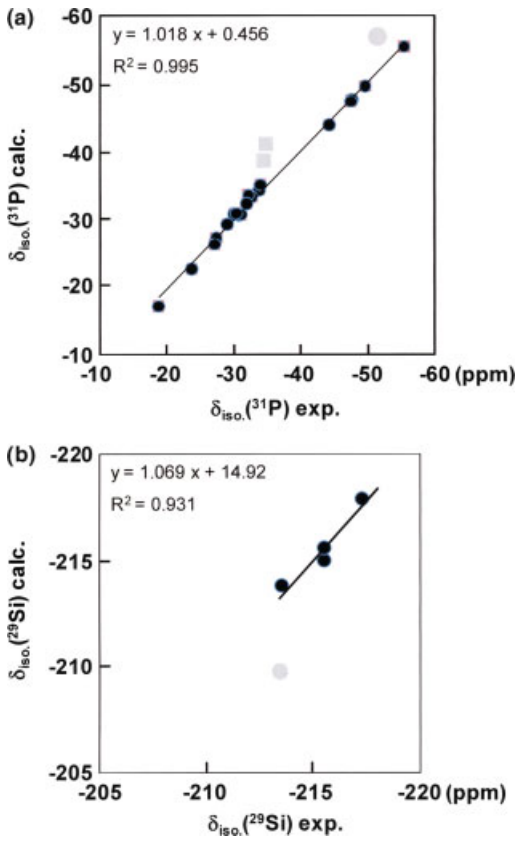

Figure 3. (a) GIPAW-calculated *versus* experimental ^{31}P isotropic chemical shifts for $Si_5O(PO_4)_6$, SiP_2O_7 polymorphs and α-, β-, γ-$Ca(PO_3)_2$ phases. Light gray squares: P4 and P5 sites in α-$Ca(PO_3)_2$.[36] Light gray circle: SiP_2O_7 hexogonal 1 form (see text). (b) GIPAW-calculated *versus* experimental ^{29}Si isotropic chemical shifts for sixfold coordinated atoms. Light gray circle: SiP_2O_7 hexogonal 1 form (see text). Experimental errors for ^{31}P and ^{29}Si NMR data are estimated to be 0.05 ppm.

As stated above, $Si_5O(PO_4)_6$ is characterized by two sixfold silicon atoms (Si1 and Si2) and one unique fourfold silicon atom (Si3). By $^{31}P \rightarrow {}^{29}Si$ MAS-J-INEPT experiments, it has been possible to study the ^{29}Si evolution *versus* the second delay of the INEPT sequence (τ').[24] The INEPT curves were fitted by using the multispin formula derived from the product operator (PO) formalism. The INEPT curves for Si1 and Si2 were shown to be different and correspond indeed to different spin systems (SI_6 for Si1 involving a unique P–O3–Si1 chemical path and SI_3I_3' for Si2 involving P–O2–Si2 and P–O5–Si2 chemical paths; see the inserts in Fig. 1a). The extracted J values were as follows: 15 Hz (±2 Hz) for Si1, $J_1 = 14$ Hz and $J_2 = 4$ Hz (±2 Hz) for Si2 and 12 Hz (±2 Hz) for Si3. The calculated values show unambiguously that strongly different $^2J_{P-O-Si}$ are expected for Si2 (−16.22 and −1.17 Hz, respectively, Table 3). This result is in full agreement with the experimental INEPT data. It has to be noticed that P–O2–Si2 is approximately 131° and P–O5–Si2 is approximately 151°. This could explain the strong difference between J_1 and J_2. Several comments have to be added. First, the sign of the J coupling constants is calculated by PAW. By using echo techniques, the absolute sign of J cannot be measured. We are currently thinking about NMR pulse schemes that would be sensitive to the sign of J by using off-MAS experiments (Ref. [55] and S. Wimperis, Private communication). Secondly, a drastic increase of $^1J_{P-O}$ is observed when considering P–O5 (factor of ~2; Table 4). Again, the P–O5–Si_2 chemical bond path seems to be quite unusual from the J coupling constants point of view. The order of magnitude of the calculated $^1J_{P-O}$ constants is in agreement with data already published in the literature (see for instance ~150 Hz for a P=O double bond in Ph_3PO).[56]

In the case of SiP_2O_7 polymorphs, calculations were performed for three different structures: two monoclinic forms AIII and AIV and one hexagonal, hexogonal 1. The calculated J data are presented in Table 3 and Fig. 4, showing the scattering of the $^2J_{P-O-Si}$ values. In terms of P–O–Si bond paths, both monoclinic forms AIII and AIV correspond to 'the worst case' with six different chemical bonds (O2 → O7). Moreover, one observes a continuum of J couplings starting from −3.18 to −12.64 Hz.

Using the PO formalism and six different isotropic J values ($J_1, \ldots, J_6$), one finds[24] (taking only the heteronuclear coupling constants):

$$I_{INEPT}(\tau,\tau') = I_0(\cos(2\pi J_3\tau')\ \cos(2\pi J_4\tau')\ \cos(2\pi J_5\tau')\ \cos(2\pi J_6\tau')$$
$$[\sin(2\pi J_1\tau)\ \sin(2\pi J_1\tau')\ \cos(2\pi J_2\tau') + \sin(2\pi J_2\tau)\ \sin(2\pi J_2\tau')$$
$$\cos(2\pi J_1\tau')] + \cos(2\pi J_1\tau')\ \cos(2\pi J_2\tau')\ \cos(2\pi J_5\tau')\ \cos(2\pi J_6\tau')$$
$$[\sin(2\pi J_3\tau)\ \sin(2\pi J_3\tau')\ \cos(2\pi J_4\tau') + \sin(2\pi J_4\tau)\ \sin(2\pi J_4\tau')$$
$$\cos(2\pi J_3\tau')] + \cos(2\pi J_1\tau')\ \cos(2\pi J_2\tau')\ \cos(2\pi J_3\tau')\ \cos(2\pi J_4\tau')$$
$$[\sin(2\pi J_5\tau)\ \sin(2\pi J_5\tau')\ \cos(2\pi J_6\tau') + \sin(2\pi J_6\tau)\ \sin(2\pi J_6\tau')$$
$$\cos(2\pi J_5\tau')]) \times \exp(-2\tau/T_2'(^{31}P))\ \exp(-2\tau'/T_2'(^{29}Si)) \quad (1)$$

By using various sets of ($J_1, \ldots, J_6$) coupling constants, it is possible to estimate the impact of each constant on a given INEPT curve for fixed τ value and variable τ' (T_2' constants were measured independently: $T_2'(^{29}Si) \sim 70$ ms, $T_2'(^{31}P) \sim 40$ ms). We focus first on mono. AIII and mono. AIV ($\delta_{29Si} = -215.1$ ppm). The experimental INEPT curve is presented in Fig. 5a (for the sum of AIII and AIV contributions). The evolution for τ' varying from 0 to 35 ms corresponds to a rapid increase of magnetization (max. at $\tau' \sim 8$ ms) followed by a slower decay (to almost 0 at $\tau' \sim 30$ ms). Several models (using Eqn (1)) are shown: all $J = -3.18$ Hz, corresponding to the lowest calculated $|^2J_{P-O-Si}|$, all

Table 2. GIPAW-calculated ^{17}O parameters for $Si_5O(PO_4)_6$ (quadrupolar constant, C_Q, in megahertz; asymmetry parameter, η_Q; see the Experimental section for definitions of C_Q and η_Q)

Phases	Sites	Coordinence	δ_{iso} (ppm) Calculated	δ_{11} (ppm) Calculated	δ_{22} (ppm) Calculated	δ_{33} (ppm) Calculated	C_Q (MHz) Calculated	η_Q Calculated
$Si_5O(PO_4)_6$	O_1	Si_{IV}–O–Si_{IV}	37.8	62.9	62.9	−12.3	−6.1	0.0
	O_2	P–O–Si_{VI}	116.0	151.2	133.7	63.2	−6.7	0.4
	O_3	P–O–Si_{VI}	103.0	136.2	126.2	46.5	−7.3	0.2
	O_4	P–O-Si_{IV}	71.3	108.2	98.6	7.1	−7.2	0.2
	O_5	P–O–Si_{VI}	96.7	132.3	119.8	38.0	−7.5	0.1

Table 3. PAW-calculated $^{2}J_{P-O-Si}$ coupling constants for $Si_5O(PO)_4$[11] and SiP_2O_7 polymorphs (mono. AIII, mono. AIV, hexogonal 1)

		Ramsey Terms (Hz)				Principal components (Hz)				
	r (angle)	FC	SD	PARA	Dia	J_{11}	J_{22}	J_{33}	J_{iso} (Hz)	J_{aniso} (Hz)
AIII										
P1–O4–Si	3.063	−2.90	0.05	−0.21	−0.11	0.60	−1.73	−8.40	−3.18	−7.84
P2–O7–Si	3.074	−4.98	0.07	−0.18	−0.11	−2.64	−3.76	−9.20	−5.20	−6.00
P1–O3–Si	3.092	−4.72	0.08	−0.10	−0.12	−1.59	−3.87	−9.11	−4.86	−6.38
P2–O6–Si	3.127	−8.30	−0.07	−0.22	−0.11	−4.47	−5.52	−16.14	−8.71	−11.14
P1–O2–Si	3.141	−6.33	−0.14	−0.16	−0.11	−2.32	−3.89	−13.98	−6.73	−10.87
P2–O5–Si	3.161	−11.81	−0.39	−0.35	−0.09	−4.03	−9.87	−24.02	−12.64	−17.07
AIV										
P1–O3–Si	3.063	−8.12	0.13	−0.10	−0.12	−4.90	−7.61	−12.12	−8.21	−5.87
P2–O5–Si	3.093	−5.52	−0.01	−0.30	−0.11	−1.81	−3.87	−12.14	−5.94	−9.31
P2–O6–Si	3.099	−7.01	0.03	−0.17	−0.11	−3.33	−5.73	−12.72	−7.26	−8.20
P2–O7–Si	3.113	−7.57	−0.11	−0.27	−0.11	−3.66	−5.43	−15.09	−8.06	−10.55
P1–O2–Si	3.128	−4.95	0.00	−0.13	−0.11	−1.42	−3.42	−10.73	−5.19	−8.31
P1–O4–Si	3.190	−4.72	−0.53	−0.31	−0.09	0.31	−0.42	−16.84	−5.65	−16.79
Hexogonal 1										
P1–O1–Si	3.073	−6.52	0.06	−0.26	−0.05	−3.13	−5.53	−11.65	−6.77	−7.31
$Si_5O(PO_4)_6$										
P–O2–Si2	–	–	–	–	–	–	–	–	−16.22	–
P–O3–Si1	–	–	–	–	–	–	–	–	−17.08	–
P–O4–Si3	–	–	–	–	–	–	–	–	−14.18	–
P–O5–Si2	–	–	–	–	–	–	–	–	−1.17	–

The definitions of J_{ii} and J_{aniso} are given in the Experimental section.

Table 4. PAW-calculated $^{1}J_{P-O}$ coupling constants for $Si_5O(PO)_4$[11] and SiP_2O_7 polymorphs (mono. AIII, mono. AIV, hexogonal 1)

		Ramsey terms (Hz)				Principal components (Hz)				
	r (angle)	FC	SD	PARA	DIA	J_{11}	J_{22}	J_{33}	J_{iso} (Hz)	J_{aniso} (Hz)
AIII										
P2–O5	1.504	17.49	−0.37	20.85	−0.33	98.65	96.65	−82.38	37.64	−180.02
P2–O6	1.512	47.58	−0.52	21.93	−0.33	133.54	128.06	−55.62	68.66	−186.42
P2–O7	1.512	54.51	−1.02	22.94	−0.33	147.55	136.27	−55.52	76.10	−197.42
P1–O3	1.518	63.64	−1.33	22.99	−0.33	152.72	144.95	−42.75	84.97	−191.59
P1–O1	1.582	29.69	−1.37	14.11	−0.33	86.76	79.61	−40.08	42.10	−123.26
P2–O1	1.590	35.44	−0.86	13.38	−0.32	89.05	85.00	−31.12	47.64	−118.15
AIV										
P1–O4	1.502	33.20	−0.46	21.17	−0.34	117.35	108.69	−65.33	53.57	−178.35
P2–O6	1.516	57.77	−1.27	22.50	−0.33	145.90	138.71	−48.63	78.66	−190.93
P1–O2	1.518	53.54	−0.54	21.88	−0.34	138.49	132.87	−47.73	74.54	−183.41
P1–O3	1.522	50.84	−0.82	22.46	−0.33	140.06	132.65	−56.29	72.14	−192.64
P1–O1	1.586	49.97	−1.15	14.63	−0.33	108.20	102.42	−21.23	63.13	−126.53
P2–O1	1.601	47.83	−1.37	13.50	−0.33	102.47	94.63	−18.22	59.63	−116.77
Hexogonal 1										
P1–O1	1.513	44.63	−0.95	22.18	−0.28	132.84	124.46	−60.58	65.57	−189.23
P1–O2	1.553	−28.57	−0.94	12.95	−0.28	23.16	23.01	−96.66	−16.83	−119.75
$Si_5O(PO_4)_6$										
P–O2	–	–	–	–	–	–	–	–	53.10	–
P–O3	–	–	–	–	–	–	–	–	61.49	–
P–O4	–	–	–	–	–	–	–	–	58.73	–
P–O5	–	–	–	–	–	–	–	–	103.73	–

The definitions of J_{ii} and J_{aniso} are given in the Experimental section.

Table 5. PAW-calculated $^{1}J_{Si-O}$ coupling constants for SiP_2O_7 polymorphs (mono. AIII, mono. AIV, hexogonal 1)

		Ramsey terms (Hz)				Principal components (Hz)				
	r (Ang)	FC	SD	PARA	DIA	J_{11}	J_{22}	J_{33}	J_{iso} (Hz)	J_{aniso} (Hz)
AIII										
Si–O5	1.735	17.88	0.28	−2.56	0.15	3.25	3.85	40.15	15.75	36.60
Si–O4	1.750	8.13	0.32	−2.59	0.15	−7.24	−5.84	31.11	6.01	37.65
Si–O6	1.768	11.54	0.44	−2.34	0.14	−2.58	−1.52	33.47	9.79	35.53
Si–O2	1.770	6.87	0.39	−2.22	0.14	−6.39	−5.80	27.75	5.19	33.85
Si–O7	1.777	7.93	0.31	−2.26	0.14	−5.72	−5.12	29.20	6.12	34.62
Si–O3	1.795	3.48	0.36	−2.12	0.14	−9.52	−8.58	23.68	1.86	32.74
AIV										
Si–O4	1.744	16.99	0.26	−2.43	0.15	3.18	3.73	38.00	14.97	34.54
Si–O5	1.750	11.70	0.28	−2.59	0.15	−3.26	−2.74	34.63	9.54	37.63
Si–O7	1.759	12.82	0.42	−2.40	0.14	−1.57	−1.03	35.57	10.99	36.87
Si–O6	1.778	11.39	0.27	−2.35	0.14	−2.60	−1.50	32.45	9.45	34.49
Si–O3	1.784	2.49	0.30	−2.22	0.14	−10.85	−10.03	23.01	0.71	33.46
Si–O2	1.793	4.38	0.50	−2.07	0.14	−8.96	−7.31	25.12	2.95	33.26
Hexogonal 1										
Si–O1	1.763	7.93	0.33	−2.33	0.12	−6.17	−5.28	29.60	6.05	35.32

The definitions of J_{ii} and J_{aniso} are given in the Experimental section.

Table 6. PAW-calculated $^{2}J_{P-O-P}$ coupling constants for SiP_2O_7 polymorphs (mono. AIII, mono. AIV, hexogonal 1)

		Ramsey terms (Hz)				Principal components (Hz)				
	r (angle)	FC	SD	PARA	DIA	J_{11}	J_{22}	J_{33}	J_{iso} (Hz)	J_{aniso} (Hz)
AIII										
P1–O1–P2	2.969	2.27	0.03	0.26	0.25	−3.35	−1.76	13.56	2.82	16.12
AIV										
P1–O1–P2	2.906	−7.37	−0.28	0.14	0.29	−11.03	−9.65	−1.01	−7.23	9.34
Hexogonal 1										
P1–O2–P2	3.105	14.12	2.57	0.95	0.05	1.18	1.20	50.71	17.70	49.52

The definitions of J_{ii} and J_{aniso} are given in the Experimental section.

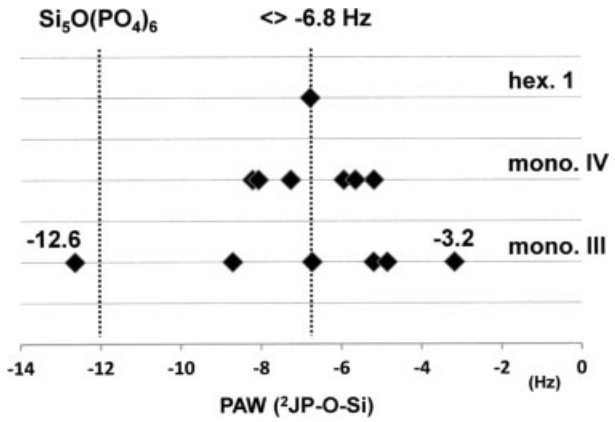

Figure 4. PAW-calculated $^{2}J_{P-O-Si}$ isotropic coupling constants for $Si_5O(PO_4)_6$, and mono. III, mono. IV and hexogonal 1 SiP_2O_7 polymorphs.

$J = -12.64$ Hz, corresponding to the highest calculated $|^{2}J_{P-O-Si}|$, $J_1 = -3.18$ Hz (×3) and $J_2 = -12.64$ Hz (×3). Obviously, the proposed models are not in agreement with the experimental data. By using Eqn (1), it is also possible to take into account the six *J* constants calculated for mono. AIII and mono. AIV. The corresponding simulations are denoted *exact* hereafter (Fig. 5b). Moreover, the arithmetic average value of the various *J*'s is estimated to −6.8 Hz for both mono. AIII and mono. AIV. The simulated INEPT curve using $J = -6.8$ Hz and Eqn (1) is also presented in Fig. 5b. The three simulated curves are in overall agreement with the experimental data. As a conclusion, there is no contradiction between the INEPT data and the PAW-calculated *J* values. The overall agreement between experimental and calculated data can be considered as good. At this stage, it does not seem possible to estimate more precisely the various *J* constants. Experiments including selective irradiations could be an alternative.[57] For the ^{29}Si resonance located at −212.8 ppm (tetragonal + hexogonal 1), the INEPT evolution (not shown here) is comparable. The maximum of the curve is located at $\tau' \sim 11$ ms and the magnetization is still positive at $\tau' = 35$ ms. As $J \sim -6.8$ Hz for hexogonal 1, it tends to suggest that $|J| \leq 6.8$ Hz for the tetragonal form. As no crystallographic data are available for the tetragonal form, this point remains an assumption.

Several comments can be added on Table 3–6. First of all, it is clearly demonstrated that the FC contribution is dominant for $^{2}J_{P-O-Si}$ and $^{2}J_{P-O-P}$, whereas the PARA term contributes

significantly to $^1J_{P-O}$ and $^1J_{Si-O}$ coupling constants (SiP_2O_7 polymorphs). Moreover, it is shown that J_{aniso} values are usually significant for all considered ^1J and ^2J coupling constants. Adequate pulse sequences have to be designed for the accurate measurement of these anisotropic components. The computed $^1J_{Si-O}$ values (Table 5) are generally smaller than $^1J_{P-O}$ even taking into consideration the fact that γ_P is twice the magnitude of $|\gamma_{Si}|$. Curiously, with the exception of $^1J_{P1-O2}$ in the hexagonal form, $^1J_{P-O}$ and $^1J_{Si-O}$ have the same sign, despite γ_P and γ_{Si} having opposite signs. We also note that the calculated $^2J_{P-O-P}$ values (Table 6) for mono. AIII and mono. AIV are of opposite signs. As mentioned above, off-MAS echo experiments could be of great help for confirming these observations.

Antisymmetric components of shift tensors in cyclopropene derivatives

We focus first here on experimental and calculated data related to cyclopropene (C_3H_4) and two of its derivatives[58] (Fig. 6 and Table 7). The calculated symmetric ^{13}C shift principal components δ_{ii} ($i = 1 \rightarrow 3$) are in good agreement with experimental data[59]: $\delta_{ii,exp} = 239$, 79 and 5 ppm for C=C and 40, 29, −59 ppm for CH_2. The GIPAW values are more accurate than those obtained by individual gauge for localized orbitals (IGLO) calculations,[58a] especially for δ_{33}(C=C) (i.e. 293 ppm). The C_{2v} symmetry for $^{13}CH_2$ and C_s symmetry for ^{13}C=C impose $\delta_{ij,i\neq j} = 0$ ($i,j = 1$, 2, 3), and $\delta_{12} \neq 0$, respectively.[13] These predictions are in full agreement with calculated data (Table 7). It follows that $A^2 = \Sigma(\delta_{ij})^2 = (\delta_{12})^2$ for cyclopropene and C_3X_4 (X = Cl, F) derivatives. The A parameter obtained by GIPAW is 88.4 ppm, whereas IGLO calculations lead to $A = 139.4$ ppm.[58a] In the case of C_3Cl_4, Anet *et al.*[15] have estimated the A and S parameters by performing variable temperature T_1 and T_2 measurements: $S \sim 150$ ppm and $A \sim 50$ ppm. The GIPAW calculations lead to $S = 160.7$ ppm and $A = 60.1$ ppm, which are in excellent agreement with experimental data. Again, the GIPAW data seem more accurate that CHF (coupled Hartree–Fock) and IGLO

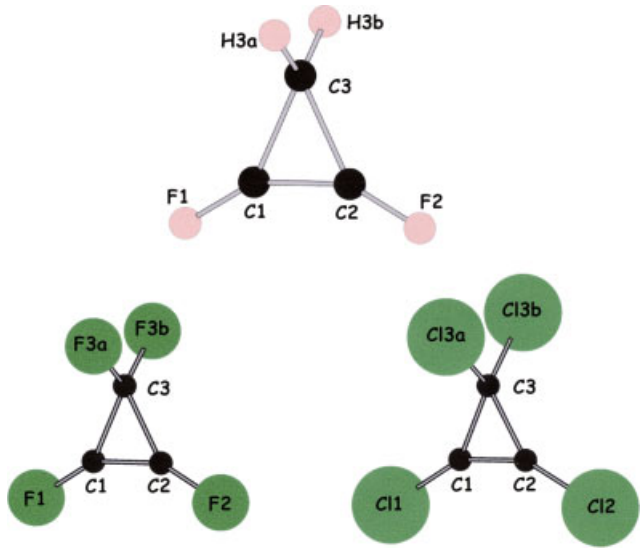

Figure 6. Molecular representation of C_3X_4 derivatives (X = H, Cl, F). CIF files are given in SI.

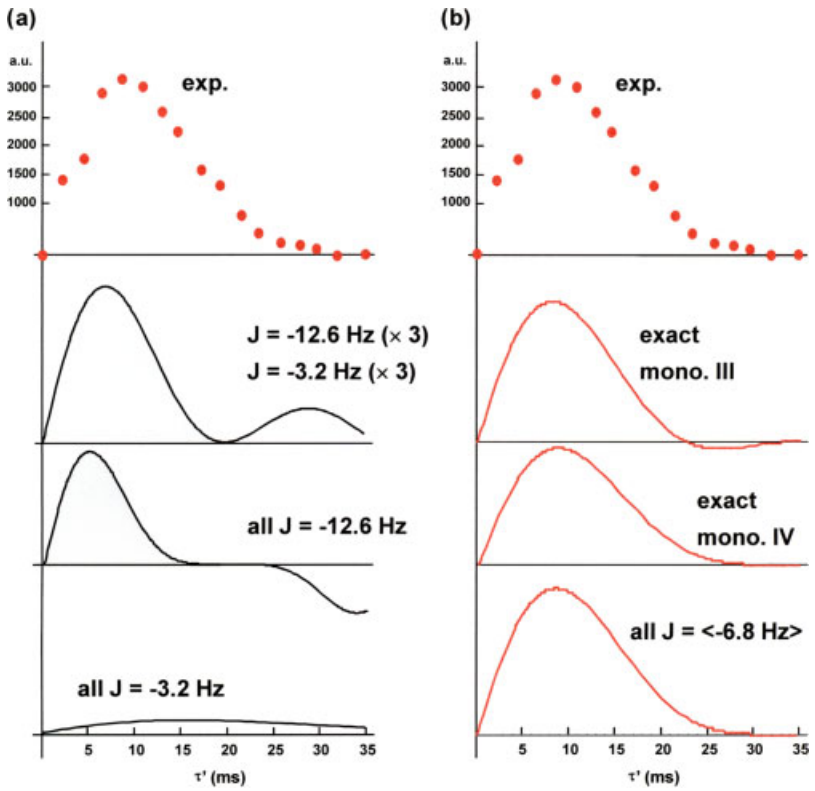

Figure 5. (a) $^{31}P-^{29}Si$ MAS-J-INEPT experimental data for mono. III and mono. IV SiP_2O_7 polymorphs (dotted line). The simulations (solid lines) correspond to Eqn (1) with various sets of ($J_1, \ldots, J_6$) constants. The 'exact' simulations use the six coupling constants given in Table 3. In (b), the scaling of the red curves is arbitrary.

Table 7. GIPAW-calculated antisymmetric shift tensor components for C_3X_4 (X = H, F, Cl)

	δ_{iso}	δ_{11}	δ_{22}	δ_{33}	δ_{12}	S	A	δ_{CSA}	η
Cyclopropene									
C1/C2	110.8	−6.6	83.8	255.1	88.4	230.2	88.4	216.5	0.6
C3	−6.3	37.0	24.4	−80.2	0.0	111.5	0.0	−110.9	0.2
Cyclopropene – relaxed structure									
C1/C2	111.9	−7.8	85.1	258.5	90.4	234.1	90.4	219.8	0.6
C3	−5.3	38.3	24.5	−78.7	0.0	110.7	0.0	−110.1	0.2
Tetrafluorocyclopropene									
C1/C2	111.0	65.1	93.3	174.7	38.8	98.6	38.8	95.5	0.4
C3	98.9	70.4	86.7	139.5	0.0	62.5	0.0	60.9	0.4
Tetrafluorocyclopropene – relaxed structure									
C1/C2	112.7	66.7	95.7	175.7	38.5	97.8	38.5	94.5	0.5
C3	103.6	75.8	90.1	144.8	0.1	63.1	0.1	61.9	0.3
Tetrachlorocyclopropene									
C1/C2	124.0	48.9	92.5	230.6	59.2	164.3	59.2	159.9	0.4
C3	70.7	112.9	93.9	5.2	0.0	99.6	0.0	−98.2	0.3
Tetrachlorocyclopropene – relaxed structure									
C1/C2	127.3	65.7	104.1	242.1	60.1	160.7	60.1	157.2	0.4
C3	75.4	131.3	104.9	19.9	0.0	100.8	0.0	−98.2	0.4

The definitions of *A* and *S* are given in the Experimental section.

calculations[58b,f] ($S \sim 180$ ppm and $A \sim 67$ ppm in Ref. [58b], $S \sim 250$ ppm and $A \sim 80$ ppm in Ref. [58f]). In the case of C_3F_4, no experimental data are available, but $S = 97.8$ ppm and $A = 38.5$ ppm values (Table 7) are comparable to those calculated by Smith *et al*.[58e]

The ^{13}C, ^{1}H, ^{19}F and ^{35}Cl chemical shift data are presented in Supporting Information for the three cyclopropene-derived structures. To the best of our knowledge, only a few related ^{13}C data have been published so far in the literature ($\delta_{13C}(C_3Cl_4) = 122.3$, 62.2 ppm[15,60]). The unusual discrepancies between ^{13}C GIPAW and experimental data[61] (~7 ppm for C_3X_4, X = H, Cl) are obviously related to the used crystallographic models: as stated above, a unique C_3X_4 molecule is considered in the structure without any interaction with others.

From a spectroscopic point of view, Wi and Frydman[16] have proposed a detailed analysis of cross-correlation Hamiltonian $H^{(2)}_{Q,\sigma\,anti.}$ effects. It is predicted that antisymmetric chemical shift (ACS)/quadrupolar effects in spectra of quadrupolar nuclei can be estimated by approximately $(\delta_{ij}\omega_0)\omega_Q/\omega_0$ (where ω_Q and ω_0 stands for the quadrupolar coupling and Zeeman frequencies, respectively). The expected magnitude is therefore of the order of ppms of the quadrupole coupling constant (and is independent of the external magnetic field). For strong δ_{ij} and ω_Q, such effects should be observable. GIPAW offers a safe option for the calculation of both δ_{ij} components and ω_Q values and should lead to selected nuclei and samples with potential ACS spectral contributions. Work is in progress for that purpose.

NQR and dynamics: ^{14}N and ^{35}Cl

GIPAW calculations were performed for three N-containing derivatives possessing explosive properties, namely: hexahydro-1,3,5-trinitro-1,3,5-triazine ($C_3H_6N_6O_6$) or RDX (α- and γ-phase); octahydro-1,3,5,7-tetranitro-1,3,5,7-tetrazocine ($C_4H_8N_8O_8$) or β-HMX; 5-nitro-2,4-dihydro-1,2,4-triazol-3-one ($C_2H_2N_4O_3$) or α-NTO. The molecular structures are presented in Fig. 7, including atom labeling. For RDX and β-HMX, respectively, six and four inequivalent N atoms exist. The molecular structure of α-NTO is characterized by four inequivalent $C_2H_2N_4O_3$ molecules, leading to 16 inequivalent N atoms. In the case of RDX, two structures corresponding to the α phase were considered. Choi *et al*.[37a] used room-temperature single-crystal neutron diffraction data, whereas Toupet *et al*.[37b] unpublished results, CCDC deposition number: 771019 used single-crystal X-ray data at low temperature ($T = 110$ K). These structures will be named C-RDX (Choi) and T-RDX (Toupet) hereafter (C-RDX: $R = 0.039$, T-RDX: $R = 0.033$ with $R = \Sigma(|F_o| - |F_c|)^2/\Sigma {F_o}^2$). Moreover, the γ-RDX structure corresponding to the high-pressure phase was also considered in GIPAW calculations.[37b] Two structures were considered for β-HMX corresponding to neutron diffraction data. Space groups are $P21/c$[38a] and $P21/n$[38b] ($R \sim 0.05$ for both structures). Finally, room-temperature single-crystal X-ray diffraction was used for the crystallographic structure of α-NTO.[39]

^{1}H, ^{13}C and ^{15}N solution-state NMR data have been previously reported in the literature for RDX, HMX[62] and NTO[63] and can be summarized as follows:

RDX: ^{1}H: 6.2 ppm; ^{13}C: 62.0 ppm; ^{15}N: −32.9 ppm (nitro), −198.1 ppm (amino). HMX: ^{1}H: 6.1 ppm; ^{13}C: 64.0 ppm; ^{15}N: −34.7 ppm (nitro), −199.1 ppm (amino). NTO: ^{1}H: 13.5 ppm; ^{13}C: 148.0 ppm (C-NO_2), 154.4 ppm (C═O); ^{15}N: −109.0 ppm (N(1), N), −202.0 ppm (N(2) NH), −238.0 ppm (N(4), NH), −30.0 ppm (N(6), nitro).

GIPAW calculations for ^{1}H, ^{13}C and ^{15}N nuclei are presented in Table 8. The ^{13}C isotropic chemical shifts are in very good agreement with the experimental data (for CH_2, C═O and C-NO_2 groups). ^{1}H isotropic chemical shifts of RDX and HMX (CH_2 groups) are considerably spread. Moreover, they are almost systematically smaller than the experimental solution-state value. This can be related to H-bond interactions in solid structures, which are averaged in solution. As an example, H-bonds for H1 and H2 in C-RDX are: H1···O2 = 2.61 Å, H1···O5 = 2.77 Å, H1···O3 = 2.86 Å ($\delta(H_1) = 3.9$ ppm); H2···O4 = 2.21 Å, H2···O2 = 2.27 Å, H2···O1 = 2.48 Å ($\delta(H_2) = 6.7$ ppm). The deshielding of H2 is obviously related to short H···O contacts.[47b] It has to be noticed that δ_{1H} is highly sensitive to the structural model used for calculations (Table 8 and the ^{1}H data for C-RDX and T-RDX). In other words, it implies that high-resolution ^{1}H MAS experiments could be of great help for the validation of the proposed structures.

The calculated ^{15}N isotropic chemical shifts are also in very good agreement with experimental data, except for NO_2 groups. In that particular case, δ_{15N} are generally underestimated by approximately 20 ppm. However, it has to be noted that the T-RDX structure leads to NO_2 shifts in quite good agreement with solution-state NMR data. This structure exhibits actually the best *R* factor (see above).

Let us turn now to the theoretical calculation of the quantity C_Q, the so-called quadrupole coupling constant, and the quantity η_Q, the asymmetry parameter. Both quantities have been defined in the section 'Computational Method'. For a spin $I = 1$ (here, ^{14}N), three spin states exist defined by the eigenvalues of the spin operator I_z: $|1>$, $|0>$ and $|-1>$. If $\eta_Q = 0$ (tensor of axial symmetry), these spin states are still eigenstates of the quadrupolar Hamiltonian with however a degeneracy of the two states $|1>$ and $|-1>$. As a consequence, only one transition is observed in pure NQR (Fig. 8, left) at a frequency ν_Q defined by:

$$\nu_Q = \frac{3}{4}|C_Q| \qquad (2)$$

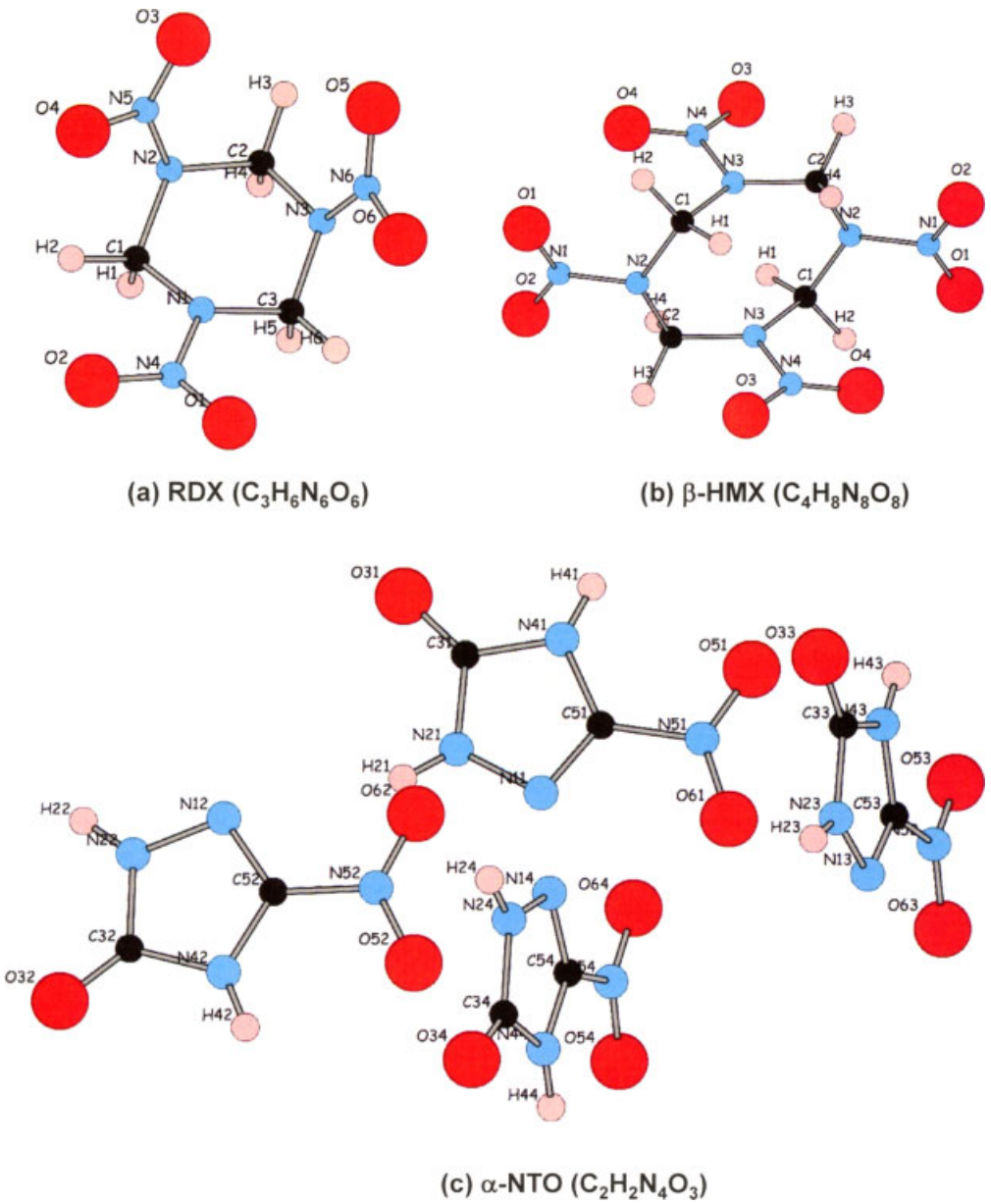

Figure 7. Molecular representation of (a) RDX, (b) β-HMX and (c) α-NTO.

However, when $\eta_Q \neq 0$, the two states $|1>$ and $|-1>$ are no longer eigenstates of the quadrupolar Hamiltonian and the eigenvectors become $2^{-1/2}(|1> + |-1>)$ and $2^{-1/2}(|1> - |-1>)$. As a consequence, three lines are observed[21] at frequencies (Fig. 8, right):

$$\nu_{\pm} = \nu_Q\left(1 \pm \frac{\eta_Q}{3}\right) \quad (3)$$

$$\nu_0 = \nu_Q\left(\frac{2}{3}\eta_Q\right) \quad (4)$$

RDX has been extensively studied by ^{14}N NQR spectroscopy, including variable temperature experiments.[64–67] For this compound (Fig. 7), the three amine atoms N1, N2 and N3 produce a total of nine resonances. Generally, the six $\nu_{\pm}$ resonances have been reported in the literature with a few exceptions for ν_0 (this can be explained by the fact that it is the lowest frequency and consequently difficult to measure for sensitivity reasons).[64,67] From their NQR experiments, Karpowicz and Brill[64] reported the following resonances for α-RDX at room temperature.

$\nu_+ = 5.240, 5.192, 5.047$ MHz, $\nu_- = 3.458, 3.410, 3.359$ MHz, $\nu_0 = 1.782, 1.688$ MHz (two lines accidentally coincide at 1.688 MHz). These values are comparable to those obtained by Ostafin ad Nogaj[65] and Ferrari.[67] It has to be noticed that Ferrari recorded the three low-frequency ν_0 resonances at 1.7851, 1.7845 and 1.6912 MHz.

The calculations related to the C-RDX and T-RDX structures (Table 8) indicate that (i) the (C_Q, η_Q) are almost identical for N1, N2 and N3 in C-RDX. This seems to be in contradiction with the experimental data. On the other hand, the T-RDX structure leads to distinct C_Q values. Moreover, the prediction of the $\delta_{15N}(NO_2)$ is more accurate for T-RDX (see above). It follows that the T-RDX model is probably more accurate that C-RDX; (ii) starting from

T-RDX, the three sets of calculated parameters (C_Q, η_Q) for N1, N2 and N3 correspond to $\nu_+ = 5.47, 5.29, 4.68$ MHz, $\nu^- = 3.60, 3.58, 3.44$ MHz, $\nu_0 = 1.88, 1.71, 1.24$ MHz, respectively. These values are globally overestimated when compared to room-temperature data (see above), as all GIPAW calculations are performed at 0 K. It is well known that the temperature dependence of the NQR resonances originates in the librational motions of the molecules in the crystal structure[21] causing a partial averaging of the EFG. Following Bayer's theory[68], the NQR resonances can be evaluated in a first approximation by using the following equation[65]:

$$\nu_Q(T) = \frac{a - b}{[\exp(c/T) - 1]} \quad (5)$$

where a is the NQR frequency extrapolated at 0 K (rigid lattice). Usually, a, b and c coefficients are extracted from the fitting of the $\nu_Q(T)$ curves in a given range of temperature. Karpowicz and Brill[64] have recorded the $\nu_{\pm,0}$ resonances in the range of 77–338 K. At low temperatures (<147 K), the variation of $\nu_{\pm,0}$ can be estimated as −0.200 kHz/K. Starting from the experimental data at 77 K,[64] and assuming a constant variation of −0.200 kHz/K, the following extrapolated values can be calculated: $[\nu_+]_{\to 0K} = 5.334, 5.271, 5.133$ MHz, $[\nu_-]_{\to 0K} = 3.527, 3.429, 3.409$ MHz, $[\nu_0]_{\to 0K} = 1.858, 1.822, 1.739$ MHz. These extrapolated values have to be compared to the calculated ones (see point (ii) above). An excellent agreement is observed, except for ν_+ (N3) which exhibits a deviation of ∼9% (as $\nu_+ - \nu_- = \nu_0$ by definition, a significant

Table 8. PAW- and GIPAW-calculated NMR data for RDX,[37] β-HMX[38] and α-NTO[39]

	α-RDX						γ-RDX		
	C-RDX Choi[37a]			T-RDX Toupet 2009[a]			Goto[37b]		
	δ_{iso} (ppm)	C_Q (MHz)	η_Q	δ_{iso} (ppm)	C_Q (MHz)	η_Q	δ_{iso} (ppm)	C_Q (MHz)	η_Q
O1	399.2	11.90	1.00	442.5	12.22	0.91	451.6	12.46	0.91
O2	423.8	−12.60	0.93	451.3	12.45	0.85	494.0	13.14	0.88
O3	428.0	12.38	0.86	450.3	12.56	0.96	455.2	12.34	0.85
O4	425.5	12.32	0.88	453.6	12.48	0.85	421.9	−11.49	0.98
O5	422.2	12.28	0.87	470.0	−14.07	0.79	514.5	12.56	0.72
O6	441.8	12.45	0.84	487.1	−14.49	0.75	421.2	12.56	0.87
N1	−203.8	−6.08	0.55	−178.5	−6.05	0.62	−211.5	−6.19	0.51
N2	−191.3	−6.02	0.58	−194.0	−5.91	0.58	−188.9	−5.97	0.55
N3	−194.6	−6.09	0.57	−188.7	−5.41	0.46	−204.7	−6.19	0.53
N4	−56.7	−0.74	0.81	−41.8	0.73	0.89	−66.3	−1.15	0.45
N5	−50.8	−0.61	0.98	−45.9	−0.73	0.88	−52.8	0.72	0.69
N6	−53.8	0.61	0.93	−29.8	−0.80	0.49	−52.1	−0.79	0.72
C1	56.4	–	–	55.4	–	–	61.3	–	–
C2	57.6	–	–	60.5	–	–	55.2	–	–
C3	56.6	–	–	60.2	–	–	59.7	–	–
H1	3.9	–	–	2.9	–	–	5.7	–	–
H2	6.7	–	–	4.7	–	–	6.5	–	–
H3	5.9	–	–	2.5	–	–	4.6	–	–
H4	4.4	–	–	3.5	–	–	4.0	–	–
H5	4.5	–	–	5.0	–	–	5.0	–	–
H6	4.5	–	–	3.0	–	–	8.5	–	–

	β-HMX					
	Choi[38a]			Choi (1967)[38b]		
	δ_{iso} (ppm)	C_Q (MHz)	η_Q	δ_{iso}(ppm)	C_Q (MHz)	η_Q
O1	436.3	−12.62	0.97	430.3	−12.67	0.96
O2	434.6	12.43	0.96	417.0	12.24	0.89
O3	422.3	12.30	0.91	448.5	12.63	0.97
O4	409.5	12.00	0.95	408.4	11.86	0.95
N1	−50.3	−0.86	0.58	−55.5	−0.81	0.75
N2	−196.0	−6.14	0.45	−201.0	−6.12	0.45
N3	−198.9	−6.51	0.46	−197.1	−6.43	0.47
N4	−55.7	−0.63	0.88	−50.6	−0.70	0.70
C1	62.3	–	–	61.2	–	–
C2	64.2	–	–	60.6	–	–
H1	4.5	–	–	3.4	–	–
H2	6.3	–	–	6.4	–	–
H3	5.7	–	–	6.0	–	–
H4	4.2	–	–	3.1	–	–

Table 8. (*Continued*)

	α-NTO Bolotina *et al.*[39]				
	δ_{iso} (ppm)	C_Q (MHz)	η_Q		δ_{iso} (ppm)
O31	178.2	7.08	0.85	C31	150.6
O32	173.8	7.12	0.93	C32	149.7
O33	176.3	7.07	0.90	C33	150.2
O34	175.0	7.05	0.88	C34	149.7
O51	556.6	13.39	0.62	C51	149.3
O52	556.1	13.35	0.65	C52	149.6
O53	562.7	13.44	0.61	C53	149.0
O54	549.2	13.19	0.66	C54	148.0
O61	529.1	12.97	0.68	–	–
O62	541.2	13.17	0.62	H21	11.3
O63	538.2	13.07	0.70	H22	11.1
O64	551.6	13.27	0.64	H23	11.1
				H24	11.2
N11	−118.3	−4.18	0.70	H41	11.7
N12	−114.8	−4.10	0.78	H42	11.6
N13	−115.0	−4.25	0.72	H43	11.5
N14	−114.6	−4.23	0.78	H44	11.3
N21	−199.0	−3.71	0.95		
N22	−196.1	−3.70	0.99		
N23	−198.3	−3.65	0.98		
N24	−195.7	−3.72	1.00		
N41	238.7	−2.90	0.42		
N42	−235.4	−2.84	0.49		
N43	−236.3	−2.94	0.44		
N44	−236.9	−2.92	0.43		
N51	−40.9	0.57	0.86		
N52	−44.4	0.57	0.78		
N53	−41.0	0.62	0.77		
N54	−41.1	0.62	0.79		

[a] Toupet *et al.* unpublished results, CCDC deposition number: 771019.

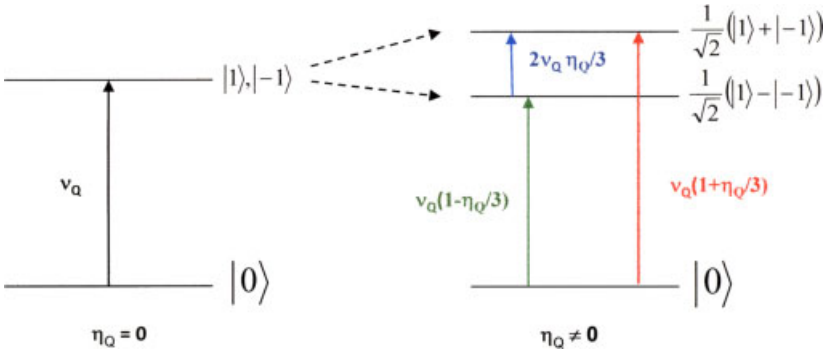

Figure 8. Energy level diagrams for pure NQR and $I = 1$ ($\eta_Q = 0$ and $\eta_Q \neq 0$).

deviation is also observed for the low frequency resonance ν_0(N3)). N1 and N2 nuclei are characterized by $\eta_Q = 0.62$ and 0.58, respectively, in very good agreement with experimental data[64] ($<\eta_Q>= 0.6196$). For N3, the combination of smaller $|C_Q|$ (=5.41 MHz) and η_Q (=0.46) (Table 8) is the main cause for the underestimation of ν_+ (N3). At this stage, we strongly believe that the T-RDX structure can be used as a safe starting point for further NMR–NQR–crystallography studies. In that particular case, $\delta_{15N}(NO_2)$ and (C_Q, η_Q) parameters (especially for N3) could act as pertinent constraints on the various calculated structural models.

The calculated GIPAW parameters for γ-RDX are comparable to those obtained for the α phase (Table 8). Indeed, structural similarities have been previously reported for both structures.[37b]

N2 and N3 atoms in β-HMX are characterized by slightly stronger $|C_Q|$ when compared to RDX (Table 8; both β-HMX structures lead to comparable NMR parameters). This trend is in agreement with

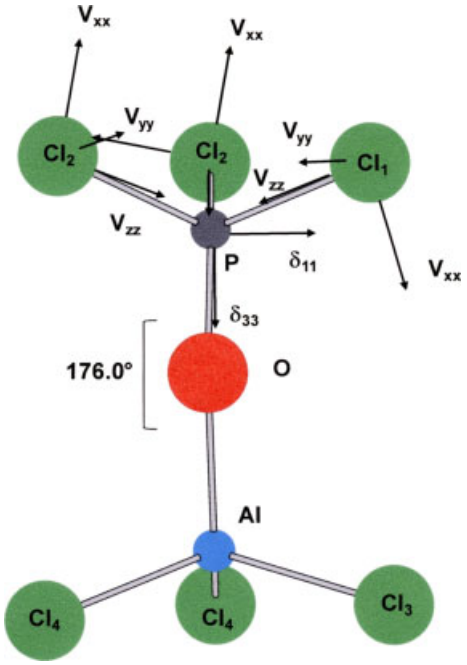

Figure 9. Molecular representation of $AlOPCl_6$.[28] The EFG tensors for Cl1, Cl2 are represented as well.

experiments.[69] Landers *et al*. performed variable temperature NQR experiments down to 77 K. Experimental $<\eta_Q>= 0.5143$, which is in good agreement with GIPAW-calculated η_Q for N2 and N3 (0.45 and 0.46, respectively). Starting from the experimental NQR resonances at 77 K and assuming a constant variation of −0.100 kHz/K, the following extrapolated values can be calculated: $[\nu_+]_{\to 0K} = 5.344$, 5.099 MHz, $[\nu_-]_{\to 0K} = 3.753$, 3.636 MHz, $[\nu_0]_{\to 0K} = 1.599$, 1.470 MHz. The GIPAW-derived results are the following: $\nu_+ = 5.57$, 5.27 MHz, $\nu_- = 4.06$, 3.90 MHz, $\nu_0 = 1.51$, 1.38 MHz. As for RDX, deviations between experimental and calculated data for $\nu_\pm$ are <7.5%. Moreover, it has to be noted that N3 exhibits the strongest $|C_Q|$, as already mentioned in the literature[69] (N3 corresponds to the 'axial' amine in the structure). The deviations between calculated and extrapolated NQR resonances are actually stronger for β-HMX than for RDX. This observation has to be related to the *R* factor of the structures: $R \sim 0.05$ for β-HMX and $R = 0.033$ for R-RDX.

The GIPAW calculations related to α-NTO are particularly interesting. N atoms are characterized by quite different (C_Q, η_Q) sets of parameters, namely:

$$\text{N11} \to \text{N14} : |C_Q| \sim 4.2 \text{ MHz},\ \eta_Q \sim 0.75,$$
$$\text{N21} \to \text{N24} : |C_Q| \sim 3.7 \text{ MHz},\ \eta_Q \sim 1.00,$$
$$\text{N41} \to \text{N44} : |C_Q| \sim 2.9 \text{ MHz},\ \eta_Q \sim 0.45.$$

The corresponding NQR frequencies are therefore:

$$\text{N11} \to \text{N14} : \nu_+ \sim 3.94 \text{ MHz},\ \nu_- \sim 2.36 \text{ MHz},\ \nu_0 \sim 1.58 \text{ MHz},$$
$$\text{N21} \to \text{N24} : \nu_+ \sim 3.70 \text{ MHz},\ \nu_- \sim 1.85 \text{ MHz},\ \nu_0 \sim 1.85 \text{ MHz},$$
$$\text{N41} \to \text{N44} : \nu_+ \sim 2.50 \text{ MHz},\ \nu_- \sim 1.84 \text{ MHz},\ \nu_0 \sim 0.65 \text{ MHz}.$$

To the best of our knowledge, no experimental NQR data for α-NTO are available in the literature. Work is in progress to detect the α-NTO NQR resonances *versus* temperature (36 lines are expected theoretically for non-NO_2 ^{14}N nuclei).

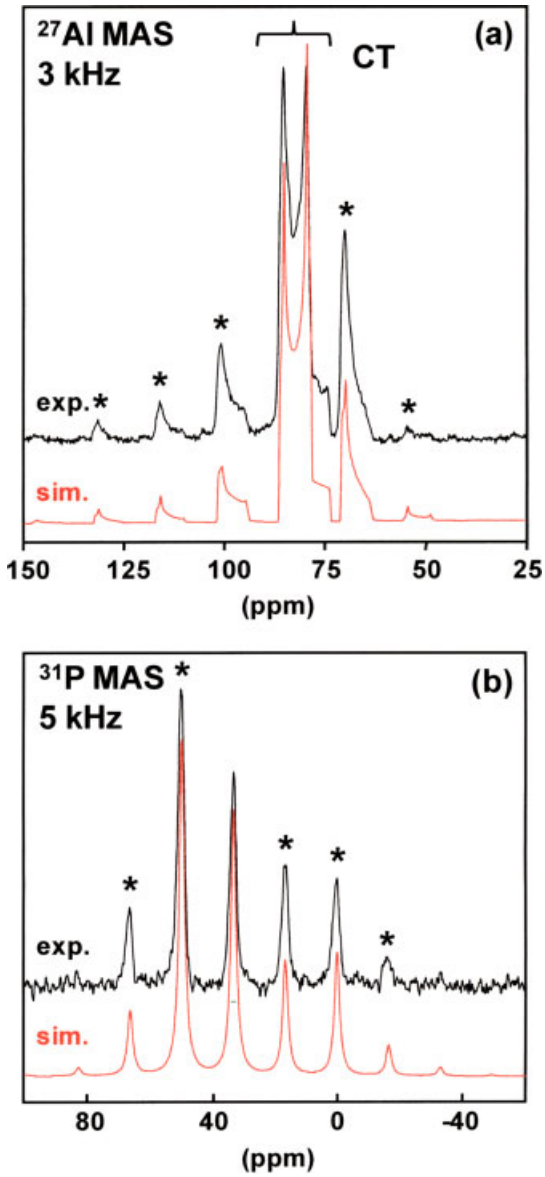

Figure 10. (a) ^{27}Al slow MAS NMR spectrum of $AlOPCl_6$. (b) ^{31}P slow MAS spectrum of $AlOPCl_6$. All NMR parameters are given in the Experimental section. CT: central transition. *: spinning sidebands. The simulated spectra were obtained by using QUASAR/DMFit.[29].

As a conclusion of this section, it has been shown that GIPAW calculations are accurate enough to predict the ^{14}N NQR resonances in explosives such as RDX and HMX. Most interestingly, GIPAW predicts also NQR resonances for γ-RDX and α-NTO, taking into account the calculated C_Q and η_Q values. This point is of paramount importance for experimentalists, especially when considering very low NQR frequencies. As an example, NO_2 groups are all characterized by small $|C_Q|$ values (~0.7 MHz) and $\eta_Q \sim 0.8$ (Table 8). The corresponding frequencies are consequently: $\nu_+ \sim 0.66$ MHz, $\nu_- \sim 0.38$ MHz, $\nu_0 \sim 0.28$ MHz. Starting from these calculated values, improvements of detection methods leading to an increase of the signal-to-noise ratio can be safely undertaken (optimization of amplifier, preamplifier, etc.).

The $AlOPCl_6$ structure is presented in Fig. 9. It is characterized by a large Al–O–P angle (176.0°). Cl1, Cl3, Al, O and P atoms lie in the same plane[28] and the molecule has near-C_{3v} sym-

Table 9. PAW- and GIPAW-calculated NMR data for $AlOPCl_6$

Phase	Sites	δ_{iso} (ppm) Calculated	δ_{11} (ppm) Calculated	δ_{22} (ppm) Calculated	δ_{33} (ppm) Calculated	C_Q (MHz) Calculated	η_Q Calculated
$AlOPCl_6$	Al	88.2	60.5	67.9	136.2	5.96	0.23
	Cl1	467.1	640.0	627.8	131.3	−54.86	0.02
	Cl2	473.4	643.8	638.6	138.0	−55.20	0.02
	Cl3	76.9	126.1	115.2	−10.4	−22.02	0.07
	Cl4	83.7	136.6	122.7	−8.3	−21.32	0.00
	O	141.7	145.1	144.0	136.0	−5.58	0.01
	P	34.5	60.1	59.5	−16.0	–	–

metry. At very high field (here, $B_0 = 17.5$ T), CSA effects are enhanced, whereas second-order quadrupolar broadening is reduced. The slow ^{27}Al MAS spectrum of $AlOPCl_6$ is presented in Fig. 10a. The isotropic part of the central transition is characteristic for a second-order quadrupolar-broadened lineshape, and the spinning sidebands show the combined effect of CSA/quadrupolar interactions. Using the QUASAR module of the DMFit software,[29] the following CSA and quadrupolar parameters have been extracted: δ_{27Al}(iso) = 88.3 ppm, $\delta_{11} = 65.4$ ppm, $\delta_{22} = 74.2$ ppm, $\delta_{33} = 125.3$ ppm, $C_Q = 6.0$ MHz, $\eta_Q = 0.17$, $\{\varphi, \chi, \psi\}_{Q\rightarrow CSA} = \{0^\circ, 0^\circ, 0^\circ\}$.[43] These values are in excellent agreement with static ^{27}Al NMR data already reported in the literature.[70] It has to be noticed that $\eta_Q \neq 0$: this result is actually not in contradiction with the crystallographic data, as Al–O–P = 176.0°. The slow ^{31}P MAS spectrum of $AlOPCl_6$ is presented in Fig. 10b ($B_0 = 17.6$ T). The spinning sideband pattern allows us to extract the following parameters for ^{31}P: δ_{31P}(iso) = 33.3 ppm, $\delta_{11} = 59.6$ ppm, $\delta_{22} = 57.4$ ppm, $\delta_{33} = -16.4$ ppm. For the simulation of the MAS spectra, dipolar couplings have been neglected ($D_{^{31}P-^{27}Al}$ ~390 Hz, $D_{^{31}P-^{35}Cl}$ ~680 Hz, $D_{^{35}Cl-^{27}Al}$ ~340 Hz). The GIPAW-calculated data for ^{27}Al and ^{31}P are presented in Table 9, and the GIPAW Euler angles for ^{27}Al are the following: $\{\varphi, \chi, \psi\}_{Q\rightarrow CSA,GIPAW} = \{-2^\circ, -1^\circ, 2^\circ\}$. All calculated data are obviously in very good agreement with experimental data for both nuclei. The GIPAW data seem more accurate than ^{27}Al cluster calculations involving Hartree–Fock and B3LYP/DFT methods.[70,71]

The $|C_Q|$ values for ^{35}Cl (Table 9) are very strong and characteristic for Cl atoms involved in covalent Al–Cl and P–Cl bonds.[21,72] As $I = 3/2$ for ^{35}Cl, a unique pure NQR resonance is expected at[21]:

$$\nu = \frac{1}{2}|CQ|(1 + {\eta_Q}^2/3)^{1/2} \quad (6)$$

As $\eta_{Q,GIPAW} \sim 0$ for Cl1 → Cl4, $\nu \sim 1/2|C_Q|$ (or ~27.5 MHz for Cl1,2 and ~10.8 MHz for Cl3,4). All our attempts to detect NQR resonances at these frequencies at *room temperature* failed. Performing variable temperature experiments, Okuda *et al.*[73] and Jost and Schneider[74] have shown previously that the ^{35}Cl and ^{81}Br NQR resonances 'fade' out for certain temperatures in the case of $GaOPCl_6$ an $AlOPBr_6$, respectively. The disappearance of the NQR resonances can be attributed to the onset of hindered internal rotation about the O–P bond by the PCl_3 group and the O–Al bond by the $AlCl_3$ group.[21] Focusing on Cl1 and Cl2, we make the crude approximation that the ^{35}Cl quadrupolar parameters are equivalent for both nuclei (Table 9) and that the hindered rotation about the O–P bond exchanges rapidly the chlorine positions (the chlorine atoms form a quasi-equilateral triangle with Cl1–Cl2–Cl2 = 60.07°, Cl2–Cl1–Cl2 = 59.86°, Cl1–Cl2 = 3.122 Å and Cl2–Cl2 = 3.115 Å). The quadrupolar principal axes can be obtained from GIPAW calculations (Fig. 9). As a first approximation, V_{XX} components can be considered as collinear to P–O bond directions. Upon fast 120° hops, the averaged C_Q value can be easily calculated for Cl1,2[75]: $C_Q \sim 28.0$ MHz (with a change of sign) leading to the NQR resonance $\nu \sim 14.0$ MHz, instead of 27.5 MHz at 0 K (following the same approach, $C_Q \sim 10.8$ MHz and $\nu \sim 5.4$ MHz for Cl3,4, instead of 10.8 MHz at 0 K). The hindered rotation leads to a reduction of −1/2 of the quadrupolar constant. Work is in progress to detect these averaged NQR resonances at room temperature. Moreover, the hindered rotation of Cl atoms must have an impact on the ^{27}Al, ^{17}O and ^{31}P tensorial properties. For aligned Al, O and P atoms and fast 120° hops between *strictly* equivalent Cl positions, all asymmetry parameters should be zero. Experimentally (see above), $\eta_{CSA}(^{31}P) \sim 0.0$ (<0.1). Obviously, near axiality is observed for ^{27}Al tensors but $\eta_{CSA}(^{27}Al) \neq 0.0$ and $\eta_Q(^{27}Al) \neq 0.0$. These values reflect the near-C_{3v} symmetry of $AlOPCl_6$ molecules and are not in contradiction with crystallography.

Finally, we strongly believe that the detailed variable temperature NQR study of $AlOPCl_6$, $AlOPBr_6$ and $GaOPCl_6$ could open new insights into the necessary implementation of temperature in GIPAW calculations. As shown by Jost *et al.*,[74] ^{35}Cl and ^{69} Ga NQR resonances are highly sensitive to T, exhibit different behaviors *versus* T and can be safely related to hindered rotations, librations and variations of Al(Ga)–O–P angles.

Conclusion

In this paper, we have illustrated some perspectives concerning the PAW/GIPAW approach. We believe that in the near future the PAW approach for J coupling tensors (including the J_{aniso} and $\mathbf{J}^{anti}$ parts) will be used as a routine method for accurate calculations. The antisymmetric components of σ and **J** tensors can be considered as new spectroscopic data for chemists. Measuring these antisymmetric components remains an open debate. Finally, all PAW/GIPAW data act as useful constraints in NMR/NQR crystallography. We believe that variable temperature NQR could be of great help for the realistic implementation of temperature in PAW.

Acknowledgements

This study received support from the TGE RMN THC FR 3050, which is gratefully acknowledged.

Supporting information

Supporting information may be found in the online version of this article.

Magnetic Resonance in Chemistry

References

[1] A. Lesage, *Phys. Chem. Chem. Phys.* **2009**, *11*, 6876.
[2] S. E. Ashbrook, *Phys. Chem. Chem. Phys.* **2009**, *11*, 6892.
[3] C. Bonhomme, C. Coelho, N. Baccile, C. Gervais, T. Azaïs, F. Babonneau, *Acc. Chem. Res.* **2007**, *40*, 738.
[4] (a) M. Kaupp, M. Bühl, V. G. Malkin, *Calculation of NMR and EPR Parameters*, Wiley-VCH: Weinheim, **2004**; (b) H. M. Senn, W. Thiel. *Angew. Chem. Int. Ed.* **2009**, *48*, 1198 and references therein; (c) H. A. Taha, N. Castillo, D. N. Sears, R. E. Wasylishen, T. L. Lowary, P. N. Roy, *J. Chem. Theor. Comput.* **2010**, *6*, 212; (d) K. Huynh, A. J. Lough, M. A. M. Forgeron, M. Bendle, A. P. Soto, R. E. Wasylishen, I. Manners, *J. Am. Chem. Soc.* **2009**, *131*, 7905.
[5] C. J. Pickard, F. Mauri, *Phys. Rev. B* **2001**, *63*, 245101.
[6] (a) S. E. Ashbrook, L. Le Polles, R. Gautier, C. J. Pickard, R. I. Walton, *Phys. Chem. Chem. Phys.* **2006**, *8*, 3423; (b) J. W. Zwanziger, J. L. Shaw, U. Werner-Zwanziger, B. G. Aitken *J. Phys. Chem. B* **2006**, *110*, 20123; (c) R. K. Harris, S. A. Joyce, C. J. Pickard, S. Cadars, L. Emsley *Phys. Chem. Chem. Phys.* **2006**, *8*, 137; (d) M. Profeta, F. Mauri, C. J. Pickard *J. Am. Chem. Soc.* **2003**, *125*, 541; (e) D. L. Bryce, E. B. Bultz, D. Aebi, *J. Am. Chem. Soc.* **2008**, *130*, 9282; (f) F. Vasconcelos, S. Cristol, J.-F. Paul, G. Tricot, J.-P. Amoureux, L. Montagne, F. Mauri, L. Delevoye, *Inorg. Chem.* **2008**, *47*, 7327; (g) S. E. Ashbrook, A. J. Berry, J. Andrew, D. J. Frost, A. Gregorovic, C. J. Pickard, J. E. Readman, S. Wimperis, *J. Am. Chem. Soc.* **2007**, *129*, 13213; (h) J. R. Yates, S. E. Dobbins, C. J. Pickard, F. Mauri, P. Y. Ghi, R. K. Harris, *Phys. Chem. Chem. Phys.* **2005**, *7*, 1402; (i) L. Shao, J. R. Yates, J. J. Titman, *J. Phys. Chem. A* **2007**, *111*, 13126; (j) A. C. Uldry, J. M. Griffin, J. R. Yates, M. Perez-Torralba, M. D. S. Maria, A. L. Webber, M. L. L. Beaumont, A. Samoson, R. M. Claramunt, C. J. Pickard, S. P. Brown, *J. Am. Chem. Soc.* **2008**, *130*, 945; (k) R. P. Chapman, D. L. Bryce, *Phys. Chem. Chem. Phys.* **2009**, *11*, 6987; (l) L. A. O'Dell, R. W. Schurko, *Phys. Chem. Chem. Phys.* **2009**, *11*, 7069; (m) D. Laurencin, C. Gervais, A. Wong, C. Coelho, F. Mauri, D. Massiot, M. E. Smith, C. Bonhomme, *J. Am. Chem. Soc.* **2009**, *131*, 13430; (n) L. S. Cahill, J. V. Hanna, A. Wong, J. C. C. Freitas, J. R. Yates, R. K. Harris, M. E. Smith, *Chem. Eur. J.* **2009**, *15*, 9785; (o) S. Ispas, T. Charpentier, F. Mauri, D. R. Neuville, *Solid State Sci.* **2010**, *12*, 183; (p) T. Charpentier, P. Kroll, F. Mauri, *J. Phys. Chem. C* **2009**, *113*, 7917; (q) E. Zurek, C. J. Pickard, J. Autschbach, *J. Phys. Chem. A* **2009**, *113*, 4117; (r) L. A. Truflandier, F. Boucher, C. Payen, R. Hajjar, Y. Millot, C. Bonhomme, N. Steunou, *J. Am. Chem. Soc.* **2010**, *132*, 4653. This list is by far not exhaustive.
[7] (a) R. K. Harris, R. E. Wasylishen, M. J. Duer, *NMR Crystallography*, John Wiley & Sons Ltd: **2009**; (b) C. J. Pickard, E. Salager, G. Pintacuda, B. Elena, L. Emsley, *J. Am. Chem. Soc.* **2007**, *129*, 8932; (c) B. Elena, L. Emsley, *J. Am. Chem. Soc.* **2005**, *127*, 9140; (d) B. Elena, G. Pintacuda, N. Mifsud, L. Emsley, *J. Am. Chem. Soc.* **2006**, *128*, 9555; (e) D. H. Brouwer, G. D. Enright, *Phys. Chem. Chem. Phys.* **2008**, *10*, 3857; (f) D. H. Brouwer, *J. Am. Chem. Soc.* **2008**, *130*, 6306.
[8] G. M. Day, T. G. Cooper, A. J. Cruz-Cabeza, K. E. Hejczyk, H. L. Ammon, S. X. M. Boerrigter, J. S. Tan, R. G. Della Valle, E. Venuti, J. Jose, S. R. Gadre, G. R. Desiraju, T. S. Thakur, B. P. van Eijck, J. C. Facelli, V. E. Bazterra, M. B. Ferraro, D. W. M. Hofmann, M. A. Neumann, F. J. J. Leusen, J. Kendrick, S. L. Price, A. J. Misquitta, P. G. Karamertzanis, G. W. A. Welch, H. A. Scheraga, Y. A. Arnautova, M. U. Schmidt, J. van de Streek, A. K. Wolf, B. Schweizer, *Acta Crystallogr. B* **2009**, *65*, 107.
[9] E. Salager, G. M. Day, R. S. Stein, C. J. Pickard, B. Elena, L. Emsley, *J. Am. Chem. Soc.* **2010**, *132*, 2564.
[10] (a) J. Hiet, M. Deschamps, N. Pellerin, F. Fayon, D. Massiot, *Phys. Chem. Chem. Phys.* **2009**, *11*, 6935; (b) P. Florian, F. Fayon, D. Massiot, *J. Phys. Chem. C* **2009**, *113*, 2562; (c) S. Cadars, D. H. Brouwers, B. F. Chmelka, *Phys. Chem. Chem. Phys.* **2009**, *11*, 1825; (d) F. Fayon, D. Massiot, M. H. Levitt, J. J. Titman, D. H. Gregory, L. Duma, L. Emsley, S. P. Brown, *J. Chem. Phys.* **2005**, *122*, 194313; (e) F. Fayon, C. Roiland, L. Emsley, D. Massiot, *J. Magn. Reson.* **2006**, *179*, 50; (f) D. Sakellariou, S. P. Brown, A. Lesage, S. Hediger, M. Bardet, C. A. Meriles, A. Pines, L. Emsley, *J. Am. Chem. Soc.* **2003**, *125*, 4376; (g) J. P. Amoureux, J. Trebosc, L. Delevoye, O. Lafon, B. Hu, Q. Wang, *Solid State NMR* **2009**, *35*, 12.
[11] S. A. Joyce, J. R. Yates, C. J. Pickard, F. Mauri, *J. Chem. Phys.* **2007**, *127*, 204107.
[12] (a) I. Hung, A.-C. Uldry, J. Becker-Baldus, A. Webber, A. Wong, M. Smith, S. A. Joyce, J. R. Yates, C. J. Pickard, R. Dupree, S. P. Brown, *J. Am. Chem. Soc.* **2009**, *131*, 1820; (b) S. A. Joyce, J. R. Yates, C. J. Pickard, S. P. Brown, *J. Am. Chem. Soc.* **2008**, *130*, 12663.
[13] A. D. Buckingham, S. M. Malm, *Mol. Phys.* **1971**, *22*, 1127.
[14] M. Mehring, V. A. Weberuss, *Object-Oriented Magnetic Resonance*, Academic Press: London, San Diego, **2001**.
[15] F. A. L. Anet, D. J. O'Leary, C. G. Wade, R. D. Johnson, *Chem. Phys. Lett.* **1990**, *171*, 401.
[16] S. Wi, L. Frydman, *J. Chem. Phys.* **2002**, *116*, 1551.
[17] K. J. Harris, D. L. Bryce, R. E. Wasylishen, *Can. J. Chem.* **2009**, *87*, 1338.
[18] S. Rossano, F. Mauri, C. J. Pickard, I. Farnan, *J. Phys. Chem. B* **2005**, *109*, 7245.
[19] (a) J.-N. Dumez, C. J. Pickard, *J. Chem. Phys.* **2009**, *130*, 104701; (b) Y. J. Lee, B. Bingoel, T. Murakhtina, D. Sebastiani, W. H. Meyer, G. Wegner, H. W. Spiess, *J. Phys. Chem. B* **2007**, *111*, 9711; (c) E. Pauwels, T. Verstraelen, M. Waroquier, *Spectrochim. Acta A* **2008**, *69*, 1388; (d) E. Pauwels, T. Verstraelen, H. De Cooman, V. Van Speybroeck, M. Waroquier, *J. Phys. Chem. B* **2008**, *112*, 7618; (e) I. de Gortari, G. Portella, X. Salvatella, V. S. Bajaj, P. C. A. van der Wel, J. R. Yates, M. D. Segall, C. J. Pickard, M. C. Payne, M. Vendruscolo, *J. Am. Chem. Soc* **2010**, *132*, 5993.
[20] (a) J. M. Griffin, S. Wimperis, A. J. Berry, C. J. Pickard, S. E. Ashbrook, *J. Phys. Chem. C* **2009**, *113*, 465; (b) A. Soleilhavoup, M. R. Hampson, S. J. Clark, J. S. O. Evans, P. Hodgkinson, *Magn. Reson. Chem.* **2007**, *45*, S144.
[21] T. P. Das, E. L. Hahn, *Nuclear Quadrupole Resonance Spectroscopy*, Solid State Physics, Advances in Research and Applications, Academic Press: New York, London, **1958**.
[22] (a) R. D. Brown, M. P. Head-Gordon, *Mol. Phys.* **1987**, *61*, 1183; (b) P. L. Cummins, G. B. Backsay, N. S. Hush, *Mol. Phys.* **1987**, *62*, 193.
[23] (a) C. Coelho, T. Azaï s, L. Bonhomme-Coury, J. Maquet, D. Massiot, C. Bonhomme, *J. Magn. Reson.* **2006**, *179*, 114; (b) C. Lejeune, C. Coelho, L. Bonhomme-Coury, T. Azaïs, J. Maquet, C. Bonhomme, *Solid State NMR* **2005**, *27*, 242.
[24] C. Coelho, T. Azaïs, L. Bonhomme-Coury, G. Laurent, C. Bonhomme, *Inorg. Chem.* **2007**, *46*, 1379.
[25] (a) S. E. Lister, A. Soleilhavoup, R. L. Withers, P. Hodgkinson, J. S. O. Evans, *Inorg. Chem.* **2010**, *49*, 2290; (b) S. Cadars, D. Brouwer, B. Chmelka, *Phys. Chem. Chem. Phys.* **2009**, *11*, 1825.
[26] M. T. Chenon, C. Coupry, L. G. Werbelow, *J. Phys. Chem.* **1992**, *96*, 561.
[27] (a) A. N. Garroway, *Magn. Reson. Mater. Phys.* **1999**, *9*, 103; (b) K. L. Sauer, B. H. Suits, A. N. Garroway, J. B. Miller, *J. Chem. Phys.* **2003**, *118*, 5071.
[28] N. Burford, A. D. Phillips, R. W. Schurko, R. E. Wasylishen, J. F. Richardson, *Chem. Commun.* **1997**, 2363.
[29] D. Massiot, F. Fayon, M. Capron, I. King, S. Le Calvé, B. Alonso, J. O. Durand, B. Bujoli, Z. Gan, G. Hoatson, *Magn. Reson. Chem* **2002**, *20*, 70. http://www.cemhti.cnrs-orleans.fr/.
[30] PARATEC (PARAllel Total Energy Code); B. Pfrommer, D. Raczkowski, A. Canning, S. G. Louie; Lawrence Berkeley National Laboratory (with contributions from F. Mauri, M. Cote, Y. Yoon, C. Pickard and P. Haynes) for more information see www.nersc.gov/projects/paratec.
[31] (a) S. J. Clark, M. D. Segall, C. J. Pickard, P. J. Hasnip, M. J. Probert, K. Refson, M. C. Payne, *Zeit. Kristallogr.* **2005**, *220*, 567; (b) V. Milman, K. Refson, S. J. Clark, C. J. Pickard, J. R. Yates, S.-P. Gao, P. J. Hasnip, M. J. Probert, A. Perlov, M. D. Segall. *J. Mol. Struct: THEOCHEM*, **2010**, in press.
[32] J. P. Perdew, G. W. Trucks, T. A. Keith, M. J. Frisch, *J. Chem. Phys.* **1996**, *104*, 14.
[33] N. Troullier, J. L. Martins, *Phys. Rev. B* **1991**, *43*, 1993.
[34] L. Kleinman, D. Bylander, *Phys. Rev. Lett.* **1982**, *48*, 1425.
[35] (a) H. Mayer, *Monatshefte Chem.* **1974**, *105*, 46; (b) H. Makart, *Helv. Chim. Acta* **1967**, *50*, 399; (c) G. Bissert, F. Liebau, *Acta Crystallogr. B* **1970**, *26*, 233; (d) K. F. Hesse, *Acta Crystallogr. B* **1979**, *35*, 724.
[36] M. Weil, M. Puchberger, J. Schmedt auf der Günne, J. Weber, *Chem. Mater.* **2007**, *19*, 5067.
[37] (a) C. S. Choi *Acta Cryst.* **1972**, *B 28*, 2857; (b) N. Goto, H. Fujihisa, H. Yamawaki, K. Wakabayashi, Y. Nakayama, M. Yoshida, M. Koshi *J. Phys. Chem. B* **2006**, *110*, 23655.
[38] (a) C. S. Choi *Acta Cryst.* **1970**, *B 26*, 1235; (b) C. S. Choi, **1967**, Results available upon request to the authors of the present contribution.
[39] N. Bolotina, K. Kirschbaum, A. A. Pinkerton, *Acta Cryst.* **2005**, *B 61*, 577.

[40] D. M. Poojary, R. B. Borade, F. L. Campbell, A. Clearfield, *J. Solid State Chem.* **1994**, *112*, 106.
[41] M. S. Baird, K. Spencer, S. V. Krasnoshchiokov, Yu. N. Panchenko, N. F. Stepanov, G. R. De Mare, *J. Phys. Chem. A* **1998**, *102*, 2363.
[42] C. Gervais, M. Profeta, V. Lafond, C. Bonhomme, T. Azaï s, H. Mutin, C. J. Pickard, F. Mauri, F. Babonneau, *Magn. Reson. Chem.* **2004**, *42*, 445.
[43] C. Gervais, R. Dupree, K. Pike, C. Bonhomme, M. Profeta, C. J. Pickard, F. Mauri, *J. Phys. Chem. A* **2005**, *109*, 6960.
[44] C. Gervais, D. Laurencin, A. Wong, F. Pourpoint, B. Woodward, A. P. Howes, K. J. Pike, R. Dupree, F. Mauri, C. Bonhomme, M. E. Smith, *Chem. Phys. Lett.* **2008**, *464*, 42.
[45] F. Tielens, C. Gervais, J.-F. Lambert, F. Mauri, D. Costa, *Chem. Mater.* **2008**, *20*, 3336.
[46] F. Pourpoint, A. Kolassiba, C. Gervais, T. Azaïs, L. Bonhomme-Coury, C. Bonhomme, F. Mauri, *Chem. Mater.* **2007**, *19*, 6367.
[47] (a) F. Pourpoint, C. Gervais, L. Bonhomme-Coury, T. Azaïs, C. Coelho, F. Mauri, B. Alonso, F. Babonneau, C. Bonhomme, *Appl. Magn. Reson.* **2007**, *32*, 435; (b) C. Gervais, C. Coelho, T. Azaï s, J. Maquet, G. Laurent, F. Pourpoint, C. Bonhomme, P. Florian, B. Alonso, G. Guerrero, P. H. Mutin, F. Mauri, *J. Magn. Reson.* **2007**, *187*, 131; (c) S. Cadars, A. Lesage, C. J. Pickard, P. Sautet, L. Emsley, *J. Phys. Chem. A* **2009**, *113*, 902.
[48] P. Hartmann, C. Jana, J. Vogel, C. Jäger, *Chem Phys Lett.* **1996**, *258*, 107.
[49] (a) S. E. Ashbrook, M. E. Smith, *Chem. Soc. Rev.* **2006**, *35*, 718; (b) M. Profeta, F. Mauri, C. J. Pickard, *J. Am. Chem. Soc.* **2003**, *125*, 541; (c) G. Wu Prog. *Nucl. Magn. Reson. Spectrosc.* **2008**, *52*, 118; (e) J. Zhu, A. J. Geris, G. Wu, *Phys. Chem. Chem. Phys.* **2009**, *11*, 6972.
[50] B. R. Cherry, T. M. Alam, C. Click, R. K. Brow, Z. Gan, *J. Phys. Chem. B* **2003**, *107*, 4894.
[51] D. Sundholm, J. Olsen, *J. Phys. Chem.* **1992**, *96*, 627.
[52] P. Pyykko, *Mol. Phys.* **2001**, *99*, 1617.
[53] R. K. Harris, B. E. Mann, *NMR and the Periodic Table*, Academic Press: New York, **1978**.
[54] P. Pyykko, *Mol. Phys.* **2008**, *106*, 1965.
[55] (a) G. Pileo, Y. Guo, T. N. Pham, J. M. Griffin, M. H. Levitt, S. P. Brown, *J. Am. Chem. Soc.* **2007**, *129*, 10972; (b) G. Pileo, S. Mamone, G. Mollica, I. M. Montesinos, A. Gansmüller, M. Caravetta, S. P. Brown, M. H. Levitt, *Chem. Phys. Lett.* **2008**, *456*, 116.
[56] D. L. Bryce, K. Eichele, R. E. Wasylishen, *Inorg. Chem.* **2003**, *42*, 5085.
[57] S. Cadars, A. Lesage, N. Hedin, B. F. Chmelka, L. Emsley, *J. Phys. Chem. B* **2006**, *110*, 16982.
[58] (a) J. C. Facelli, A. M. Orendt, D. M. Grant, J. Michl, *Chem. Phys. Lett.* **1984**, *112*, 147; (b) M. Jaszunski, K. L. Bak, P. Jorgensen, T. Helgaker, K. Ruud, H. J. A. Jensen, *Chem. Phys. Lett.* **1993**, *204*, 608; (c) A. Barszczewicz, M. Jaszunski, K. Mamienska-Trela, T. Helgaker, P. Jorgensen, O. Vahtras, *Theor. Chim. Acta* **1993**, *87*, 19; (d) M. Jaszunski, T. Helgaker, K. Ruud, P. Jorgensen, K. L. Bak, H. Koch, *Mol. Phys.* **1995**, *85*, 671; (e) C. M. Smith, R. D. Amos, N. C. Handy, *Mol. Phys.* **1992**, *77*, 381; (f) C. van Wüllen, U. Fleischer, W. Kutzelnigg, *Mol. Phys.* **1994**, *81*, 1373.
[59] (a) K. W. Zilm, R. T. Conlin, D. M. Grant, J. Michl, *J. Am. Chem. Soc.* **1980**, *102*, 6672; (b) A. M. Orendt, J. C. Facelli, A. J. Beeler, K. Reuter, W. J. Horton, P. Cutts, D. M. Grant, J. Michl, *J. Am. Chem. Soc.* **1988**, *110*, 3386.
[60] M. J. Taylor, L.-J. Baker, *J. Raman Spec.* **1995**, *26*, 595.
[61] J. C. Johnston, R. J. Iuliucci, J. C. Facelli, G. Fitzgerald, K. T. Mueller, *J. Chem. Phys.* **2009**, *131*, 144503.
[62] (a) Z. Fang, J. Chen, F. Li, *Prop. Expl. Pyrotech.* **1997**, *22*, 314; (b) S. Bulusu, T. Axenrod, J. R. Autera, *Org. Magn. Reson.* **1981**, *16*, 52.
[63] (a) L. Fan, C. Dass, T. J. Burkey, *J. Label. Compd. Radiopharm.* **1995**, *38*, 87; (b) J. C. Oxley, J. L. Smith, K. E. Yeager *J. Energ. Mater.* **1995**, *13*, 93; (c) H. H. Licht, H. Ritter, H. R. Bircher, P. Bigler, *Magn. Reson. Chem.* **1998**, *36*, 343.
[64] R. J. Karpowicz, T. B. Brill, *J. Phys. Chem.* **1983**, *87*, 2109.
[65] M. Ostafin, B. Nogaj, *Measurement* **2007**, *40*, 43.
[66] (a) N. T. Rudakov, V. T. Mikhaltsevitch, O. P. Selchikhin *J. Phys. D* **1997**, *30*, 1377; (b) A. Hudson, A. Chongpison, D. Loganathan J. Kury, *Appl. Magn. Reson.* **2004**, *25*, 355.
[67] M. Ferrari, *Aspects fondamentaux de la Résonance Quadripolaire Nucléaire de l'azote-14 par impulsion de champ radiofréquence – Vérifications Expérimentales*, PhD thesis, University Henri Poincaré-Nancy I, France, **2008**.
[68] H. Bayer, *Z. Physik* **1951**, *130*, 227.
[69] A. G. Landers, T. B. Brill, R. A. Marino, *J. Phys. Chem.* **1981**, *85*, 2618.
[70] R. W. Schurko, R. E. Wasylishen, A. D. Phillips, *J. Magn. Reson.* **1998**, *133*, 388.
[71] GIPAW leads to $V_{ZZ} > 0$. As $Q(^{27}Al) > 0$, $C_Q > 0$ for ^{27}Al in $AlOPCl_6$. This sign is in contradiction with that previously reported in Ref. [65].
[72] E. A. C. Lucken, *Nuclear Quadrupole Coupling Constants*, Academic Press: New York, London, **1969**.
[73] T. Okuda, H. Ishihara, K. Yamada, H. Negita, *Bull. Chem. Soc. Jpn.* **1978**, *51*, 1273.
[74] J. W. Jost, R. F. Schneider, *J. Phys. Chem. Solids* **1975**, *36*, 349.
[75] (a) C. Bonhomme, J. Livage, *J. Phys. Chem. A* **1998**, *102*, 375; (b) C. Bonhomme, J. Livage, *J. Phys. Chem. A* **1999**, *103*, 460.

